Rock Mechanics and Rock Engineering (2020) 53:1495–1519
https://doi.org/10.1007/s00603-019-01977-4

BOOK REVIEW

2D and 3D Roughness Characterization

Earl Magsipoc[1] · Qi Zhao[1,2] · Giovanni Grasselli[1]

Received: 14 February 2019 / Accepted: 11 August 2019 / Published online: 10 October 2019

Abstract

The quantification of surface roughness for the purpose of linking its effect to mechanical and hydrodynamic behavior has taken many different forms. In this paper, we present a thorough review of commonly used 2D and 3D surface roughness characterization methods, categorized as statistical, fractal, and directional. Statistical methods are further subdivided into parametric and functional methods that yield a single value and function to evaluate roughness, respectively. These statistical roughness metrics are useful as their resultant outputs can be used in estimating shear and flow behavior in fractures. Fractal characterization methods treat rough surfaces and profiles as fractal objects to provide parameters that characterize roughness at different scales. The directional characterization method encompasses an approach more closely linked to shear strength and is more suitable for estimating the influence of fracture roughness on mechanical responses. Overall, roughness characterization methods provide an effective objective measure of surface texture that describe its influence on the mechanics of surfaces without requiring qualitative description.

Keywords Roughness characterization · Rock joint roughness · Aperture · Joint shear strength · Fractal roughness · Synthetic roughness

List of Symbols

$\overline{\theta^*}$	Modified apparent dip characteristic angle
$\theta^*_{\max}/(C+1)$	Directional roughness metric
A_0	Total area fraction facing queried analysis direction
A_i	Average asperity inclination
$R_{\Delta a}$	Average slope
$R'_{\Delta a}$	Average curvature
R_ku	Kurtosis
R_p	Profile roughness coefficient
R_s	Surface roughness coefficient
R_sk	Skewness
$R_{\lambda q}$	Average wavelength
S_m	Mean zero-crossing spacing
S_p	Mean peak spacing
$Z_2, R_{\Delta q}$	Textural slope parameters
$Z_3, R'_{\Delta q}$	Textural wavelength parameters
i_p	Peak dilatancy angle
α_e	Effective asperity angle
$\beta_\text{roll-off}$	Roll-off parameter
θ^*	Apparent dip angle facing queried analysis direction
σ_c	Unconfined compressive strength
σ_n	Normal stress
σ_t	Tensile stress
φ_b	Basic friction angle
φ_r	Residual friction angle
φ_sr	Surface roughness friction angle
h	Average joint height
A	Fractal amplitude parameter
ACF(τ)	Autocorrelation
ACVF(τ)	Autocovariance function
C	Fractal amplitude parameter (spectral characterization) (Sect. 3.2), directional roughness metric fitting parameter (Sect. 4)
C'	Modified directional roughness metric fitting parameter
CLA, R_a	Center-line average asperity height
D	Fractal dimension
$G(f)$	Power spectral density (PSD)
H	Hurst exponent
JCC	Joint contact state coefficient

✉ Giovanni Grasselli
Giovanni.grasselli@utoronto.ca

[1] Department of Civil and Mineral Engineering, University of Toronto, Toronto, ON, Canada

[2] Present Address: Department of Civil and Environmental Engineering, University of California, Berkeley, Berkeley, CA, USA

JCS	Joint compressive strength
JRC	Joint roughness coefficient
L	Length of profile
$P(z)$	Cumulative probability density function
$R(f)$	Aperture to surface power spectral density ratio
RMS, Z_1, R_q	Root-mean-square asperity height
$S(w)$	Standard deviation of points in roughness-length method
b	Crossover length
f	Frequency
k	Wavenumber
n	Modified apparent dip distribution parameter
$p(z)$	Amplitude probability distribution function
w	Window width for roughness-length method
x	Profile length axis
z	Profile height axis
α	Angle between triangle normal vector and queried analysis direction
β	Spectral exponent
$\gamma(k)$	Random number sequence weighting function
κ	Topothesy (Sect. 3.2), displacement-to-joint length ratio (joint contact state coefficient) (Sect. 5.1.1)
λ	Wavelength
τ	Lag distance (autocovariance) (Sect. 2.2.1), shear strength (Sect. 5.1.1)

1 Introduction

Surfaces exhibit irregular geometries which can be described as roughness. Characterization of roughness is a wide-reaching body of knowledge with implications in many disciplines that involve surface contact (e.g., tribology, precision engineering, nanotechnology, etc.) with effects on wear, friction, fluid dynamics, etc. (e.g., Thomas 1981; Bhushan et al. 1995). In rock surfaces, roughness can be estimated at the microscopic scale (Krohn and Thompson 1986; Chae et al. 2004), laboratory scale (Poon et al. 1992; Belem et al. 2000; Fardin et al. 2001, 2004; Grasselli et al. 2002; Lanaro and Stephansson 2003; Grasselli and Egger 2003), and field scale (Power et al. 1987, 1988; Renard et al. 2006; Sagy et al. 2007; Candela et al. 2009) and can affect the mechanical and hydromechanical characteristics of joints (Barton and Choubey 1977; Barton et al. 1985).

Although the effects of roughness can be considered in estimation of hydromechanical behavior of rock joints, its degree of influence varies with scale. Therefore, the scale of measurement, as a function of the measurement resolution and captured size, must be considered in roughness characterization. The International Society of Rock Mechanics (1978) describes the different scales of rock roughness using "unevenness" to describe small-scale roughness features likely to break during shearing of rock and "waviness" as large-scale roughness features that are unlikely to break during shearing. While materials can exhibit varying degrees of roughness at various scales, not all characterization methods developed can comprehensively describe the effects of scale. This work discusses a broad, but non-exhaustive list of roughness characterization methods. The assumptions these methods rely on must be well understood before they are introduced into analysis, since their suitability may be sensitive to different applications (Thomas 1981; Reeves 1985; Power and Tullis 1991).

The existence of a vast variety of roughness characterization methods is partly because there are many "dimensions" to describing surface characteristics. We discuss various methods by grouping those that share similar basic theories. In this work, we categorized these methods into statistical, fractal, and directional roughness methods. The statistical methods carry the methods directly applied to elevation data, while the fractal and directional methods require processing techniques beyond the general ideas of statistics. In Fig. 1, we provide a broad overview these methods and highlight the sections in which we describe their details. We also show several of the various relationships between these methods which are further detailed throughout this work. The variety of characterization methods can also be attributed to their development for different materials and surface creation processes. The International Organization for Standardization (ISO) codifies many parameters for both profile and surface characterization (ISO 1997, 2010). Although most parameters are derived from precision machining and mechanical wear applications, they have characterization potential for rock surfaces since they are simple and easy to use, thus, they are discussed in this work with reference on their usage, features, and limitations.

Improvements to surface measurement technology have changed the way surface roughness is characterized. Within this work, the term "2D" refers to a linear profile extracted from the surface and "3D" refers to areal altitude maps. 3D measurements have an advantage over 2D profiles since profiles may (1) misestimate the real contact areas, potentially identifying locations that have little to no effect on shear strength, and (2) exaggerate or underestimate key surface features that affect the contacts and interactions out-of-plane with the profile orientation. The real contact area, which is important for mechanical and fluid flow behavior in rock discontinuities (Whitehouse and Archard 1970; Raven and Gale 1985; Olsson and Brown 1993), is characterized by patches throughout the nominal joint surface and is always less than the total surface area as shown in direct observations with

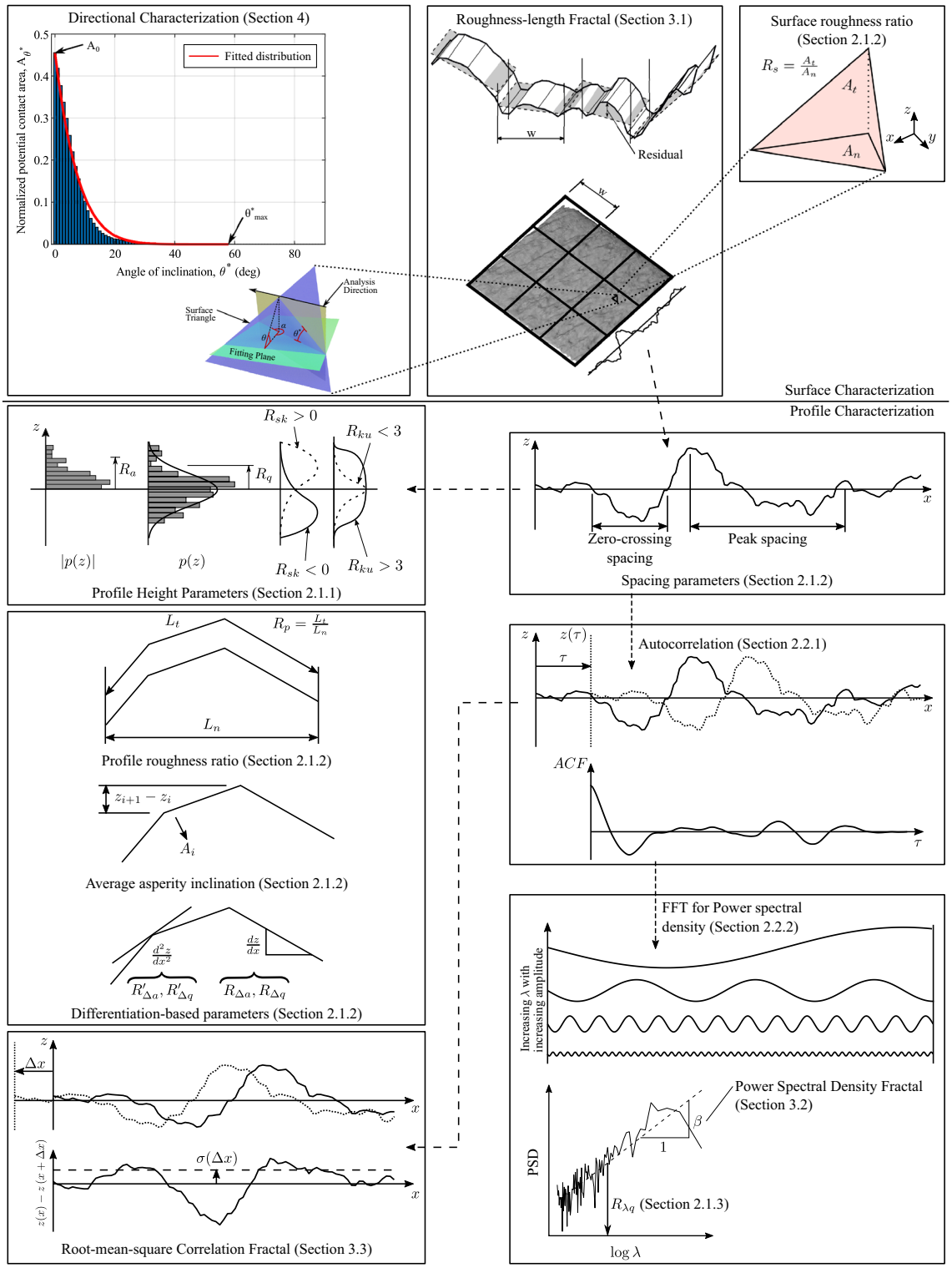

Fig. 1 Visual summary of roughness characterization described in this work

light scattering and X-ray micro-CT imaging (Dieterich and Kilgore 1994; Zhao et al. 2018) and indirect lab observations (Grasselli et al. 2002). The areal distribution and the magnitude of real contact area is also sensitive to shearing direction as a result of the directional roughness (Jing et al. 1992; Gentier et al. 2000; Belem et al. 2000; Grasselli et al. 2002).

The goal of this paper is to review surface roughness characterization methods and provide examples and insights on their usage. The applications and sensitivities of roughness characterization methods to scaling and resolution, and the prospect of measuring roughness in 3D surfaces in comparison to 2D profiles are discussed. The surface roughness characterization methods are summarized in Appendix 1, and an open-source roughness processing tool was developed and provided in Appendix 2 to ease data processing.

Throughout literature we found various inconsistencies pertaining to the terminology used for discussion, thus different variable names have also been used to refer to the same methods due to differences in naming conventions and standardization. The different variables are listed along with their description in the "List of Symbols".

2 Statistical Characterization

Although rough surfaces can have visible structural characteristics (e.g., planarity, waviness, etc.), random variability is apparent within the geometry. Statistical concepts can be applied to provide structure to a random process (e.g., surface linear profile). Prior to parameter calculation from surface measurements, in 2D, for example, the profile must be pre-processed to establish an equal sampling interval throughout the profile and to set the best-fit line of the profile as the horizontal axis (ISO 1997; Tatone 2009; Tatone and Grasselli 2010). The ISO (1997) also outlines methods to obtain mean lines for the "waviness" of profiles and "roughness" of profiles after using appropriate filters (ISO 1996), but these are not further discussed here.

2.1 Parametric Methods

Attempts to characterize roughness using a single parameter have been made to incorporate roughness into equations describing mechanical behavior (e.g., shear strength) (Tse and Cruden 1979; Maerz et al. 1990; Yu and Vayssade 1991; Yang et al. 2001; Tatone and Grasselli 2010). These parameters are typically calculated using averaging methods such as the arithmetic mean and the root-mean-square (RMS). Here, we describe various equations used to quantify roughness into a single parameter from profile (2D) measurements. Many of these parameters also have a surface (3D) analogue (ISO 2012). However, we do not discuss these in detail here since the purposes of these parameters remain the same.

2.1.1 Amplitude Parameters

When profiles are extracted from a rough surface, point elevations relative to a plane are usually measured at a set interval (e.g., profile comb measurement). Given the regularity in point measurements, an amplitude distribution function can be obtained mirroring the statistical concept of probability distribution assuming a normal distribution (Fig. 2). From the profile heights [$z(x)$], we obtain the resultant amplitude density function [$p(z)$] and cumulative amplitude density function [$P(z)$] (Fig. 2). Measures based on this concept are independent of the profile spacing length-wise and remove any localized geometric characteristics (Bhushan 2000).

The arithmetic average of the absolute height (R_a) is determined as

$$R_a = \frac{1}{L}\int_L |z|\mathrm{d}x, \tag{1}$$

where z is the distance of the profile from the mean line, or the least-squares line crossing the profile (ISO 1997), x is the length axis, and L is the length of the profile. This is complemented by the RMS of height (R_q) which is calculated as

$$R_q = \sqrt{\frac{1}{L}\int_L z^2\mathrm{d}x}. \tag{2}$$

These two parameters measure relative deviation of the profile from the mean line. While R_a is a simple average deviation, R_q provides a more familiar m elevation measure as it is essentially the standard deviation of the amplitude distribution. These two parameters are very close numerically (Krahn and Morgenstern 1979) and both describe the deviation from the mean line. The ratio of R_q/R_a is approximately 1.25 for a normal amplitude distribution but can be between 1.5 and 2.5 for a skewed height distribution (Bhushan 2000).

The profile shape can also be described using skewness and kurtosis which are the third and fourth central moments of a distribution (Fig. 3). Skewness (R_{sk}) is calculated as

$$R_{\mathrm{sk}} = \frac{1}{R_q^3}\left(\frac{1}{L}\int_L z^3\mathrm{d}x\right) \tag{3}$$

with respect to the mean line. As its name suggests, this parameter is sensitive to the symmetry of the profile about the mean line. It is particularly useful in observing general trends in peaks or valleys of the amplitude depending on the sign of the parameter. Meanwhile, kurtosis (R_{ku}) is calculated by

$$R_{\mathrm{ku}} = \frac{1}{R_q^4}\left(\frac{1}{L}\int_L z^4\mathrm{d}x\right) \tag{4}$$

and can characterize the tendency of the profile to conform with the mean line. It can also describe the difference

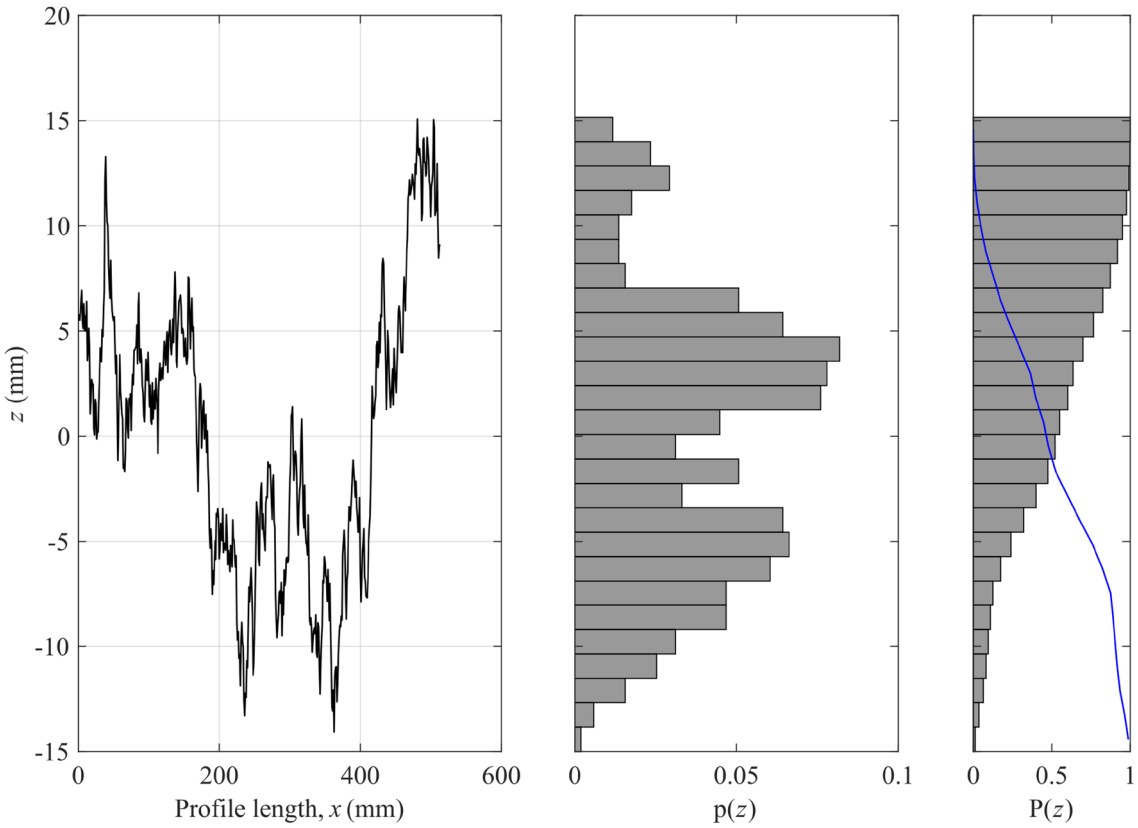

Fig. 2 A synthetic profile generated using the methodology of Candela et al. (2009) with its complementing amplitude density function, $p(z)$, and cumulative amplitude density function, $P(z)$. The line shown along with $P(z)$ is the reverse cumulative amplitude density function, $1 - P(z)$

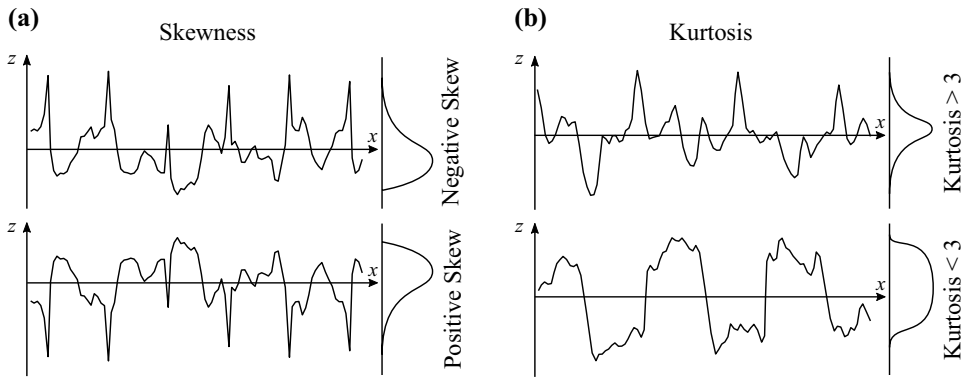

Fig. 3 The measures of skewness and kurtosis with respect to the amplitude density function provide indications of the shape of a profile. **a** The skewness is either positive or negative and determined with respect to the positive orientation of the z-axis. **b** Kurtosis corresponds to the spread along the z-axis and is compared against a normal amplitude distribution where $R_{ku} = 3$ (modified from Gadelmawla et al. 2002)

between broad and wavy or sharp and sudden peaks or valleys as a measure of profile sharpness. This parameter is referenced against the normal amplitude distribution that has $R_{ku} = 3$. The spread of the amplitude distribution is broader when $R_{ku} < 3$ and sharper when $R_{ku} > 3$. Although these parameters are occasionally referenced in the precision machining industry, they are often not used (Bhushan 2000). This is likely because they are measures of deviation from the normal distribution and may not carry significance if the profiles measured show the height distribution is close to normal distribution (Thomas 1981). They still have value in characterizing surfaces that have experienced machining processes, or permanent surface alterations, since these types of surfaces can deviate from a normal distribution (Bhushan 2000).

2.1.2 Textural (Spatial) Parameters

Amplitude parameters are too simplistic to fully describe roughness. They do not consider the local waviness and sloping of the profile, which play important roles in the mechanical behavior of surfaces. Myers (1962) proposes to estimate

roughness with Z_2 and Z_3, which are the RMS of the average local slope and average local curvature, respectively. Z_2 is mathematically described as

$$Z_2 = R_{\Delta q} = \sqrt{\frac{1}{L}\int_L \left(\frac{\mathrm{d}z}{\mathrm{d}x}\right)^2 \mathrm{d}x} \tag{5}$$

and Z_3 is

$$Z_3 = R'_{\Delta q} = \sqrt{\frac{1}{L}\int_L \left(\frac{\mathrm{d}^2 z}{\mathrm{d}x^2}\right)^2 \mathrm{d}x}. \tag{6}$$

Of these parameters, Z_2 is the most useful as the local slope was shown to be the closest roughness descriptor based on correlations to the JRC (Tse and Cruden 1979; Maerz et al. 1990; Yu and Vayssade 1991; Tatone and Grasselli 2010). However, both Z_2 and Z_3 parameters require profiles to show a persistent pattern along the mean line, or exhibit stationarity, since they are sensitive to the long-wavelength trends within the profile (Reeves 1985). This is a concern for smaller samples since non-stationarity becomes increasingly apparent as lab-scale surface samples become smaller. Filtering can be used to remove the non-stationarity and instrumentation noise affecting the results of Z_2 and Z_3 at both ends of the spectral range of roughness (Reeves 1985).

Z_2 and Z_3 are complemented by their arithmetically averaged counterparts, $R_{\Delta a}$ and $R'_{\Delta a}$, which are calculated similar to the average slope as

$$R_{\Delta a} = \frac{1}{L}\int_L \left|\frac{\mathrm{d}z}{\mathrm{d}x}\right| \mathrm{d}x \tag{7}$$

and the average curvature as

$$R'_{\Delta \mathrm{a}} = \frac{1}{L}\int_L \frac{\mathrm{d}^2 z/\mathrm{d}x^2}{\left[1+(\mathrm{d}z/\mathrm{d}x)^2\right]^{\frac{3}{2}}}\mathrm{d}x \cong \frac{1}{L}\int_L \left|\frac{\mathrm{d}^2 z}{\mathrm{d}x^2}\right| \mathrm{d}x. \tag{8}$$

As shown in Eq. (8), the calculation of $R'_{\Delta \mathrm{a}}$ can be simplified since the slope $\mathrm{d}z/\mathrm{d}x$ is usually a small value. While this may be the case for flatter profiles, rougher profiles may not experience the same simplification and the full formula should be used (Whitehouse 1994).

The average asperity inclination (A_i) is calculated by summing the vertical difference between adjacent points and dividing it by the profile length (Tatone 2009):

$$A_\mathrm{i} = \tan^{-1}\left(\frac{1}{L}\sum |z_{i+1} - z_i|\right), \tag{9}$$

where i is the index of each point. This represents an average local difference throughout the entire profile. Also, while this method is not affected by local horizontal changes in the profile, it is affected by the total profile length. This method appears similar to $R_{\Delta a}$ as they both estimate an average slope. However, the main difference is that the slope in A_i is calculated indirectly using the averaged heights while $R_{\Delta a}$ is calculated using the local segment slopes directly.

El-Soudani (1978) introduced the roughness ratio, R_p, which is the ratio of the true length of a profile to the nominal length of the profile. This is calculated as

$$R_\mathrm{p} = \frac{1}{L}\sum \sqrt{(x_{i+1} - x_i)^2 + (z_{i+1} - z_i)^2}, \tag{10}$$

where the sum of every segment length is divided by the length directly between the beginning and end points. This results in a value that will always be greater or equal to 1 with value of 1 representing a completely smooth profile. The 3D surface version of this parameter, R_s, uses surface area instead of length. This is simply calculated as

$$R_\mathrm{s} = \frac{A_\mathrm{t}}{A_\mathrm{n}}, \tag{11}$$

where A_t is the true surface area and A_n is the nominal surface area. The nominal surface area is the area of the surface after it is projected onto its best-fit plane. This characterization method is relatively simple and intuitive and it has a very close correlation with the directional roughness metric discussed in Sect. 4 (Grasselli et al. 2002; Grasselli and Egger 2003; Tatone and Grasselli 2009).

Whitehouse (1994) discusses spacing-based parameters, namely the mean peak spacing (Fig. 4a) and the mean zero-crossing spacing (Fig. 4b). These parameters are similar in that they represent an average spacing between features across a 2D profile. Mean peak spacing is defined as the average distance between peaks on a profile while the mean zero-crossing spacing is the average distance between intersections by the profile and the profile length axis (represented as the x-axis in this work) (Fig. 4).

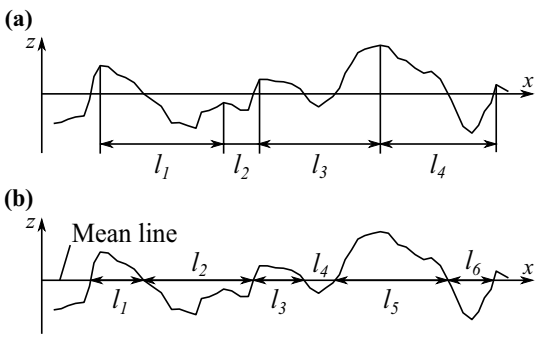

Fig. 4 **a** Selection of the peak spacing is chosen based on the presence of valleys. **b** Zero-crossing spacing is based on the intersection of the profile with the mean line (modified from Whitehouse 1994)

Whitehouse (1994) further refines the mean peak spacing concept by implementing an "amplitude discrimination band" which counts peaks that pass from the bottom to the top of the band. This filters out small peaks leaving the larger asperities on a rock surface to be the focus of the parameter.

2.1.3 Hybrid Parameters

Parameters can be combined to create new parameters that can describe both amplitude and spatial parameters. Spragg and Whitehouse (1970, 1972) proposes the use of a parameter sensitive to the wavelengths that consist the profile. The average profile wavelength ($R_{\lambda q}$) is

$$R_{\lambda q} = \frac{2\pi R_q}{R_{\Delta q}}, \tag{12}$$

where R_q is the RMS of amplitude and $R_{\Delta q}$ is the average slope of the profile. This averaged parameter is representative of the wavelengths of the entire profile and can provide a sense of the shape of the PSD function (detailed in Sect. 2.2.2) of the profile (Fig. 5). However, this parameter is likely to be sensitive to the length of the sample and the resolution used for measurement just as its components are (i.e., the domain boundaries of the PSD function).

2.2 Functional Methods

Although parameter methods have meaningful basis for their description, using single parameters may be insufficient to effectively characterize roughness (Spragg and Whitehouse 1970, 1972). In the advances made to associate roughness with mathematical theory, functional methods are often discussed. The profile changes in rough surfaces appear to be a random spatially varying process which is observable using signal processing mathematics (Whitehouse 1994). These methods are capable of representing roughness at a large range of wavelengths (Bendat 1980), and, by observing changes in functions derived from profiles, processes that affect roughness characteristics (e.g., shear, scratching, etc.) can be inferred (Rabinowicz 1956; Sayles and Thomas 1977). Several of these methods have relationships with the statistical parameters discussed earlier which helps justify the usage of both methods.

2.2.1 Autocovariance, Autocorrelation, and Structure Functions

The autocorrelation function is determined through the autocovariance function of the profile. The autocovariance function, ACVF(τ), is calculated directly from the profile as

$$\mathrm{ACVF}(\tau) = \lim_{L\to\infty} \frac{1}{L} \int_L z(x)z(x+\tau)\mathrm{d}x, \tag{13}$$

where τ is the autocovariance lag distance. This function is directly related to the autocorrelation function as $\mathrm{ACF}(\tau) = \mathrm{ACVF}(\tau)/R_q^2$,, which normalizes the autocovariance function. The limit $L \to \infty$ implies that with larger sample lengths, the function would approach values more representative of the surface; thus, whole surface should be profiled and examined when possible.

This function can help determine the correlation length which is the distance at which any two arbitrary points become statistically independent. This can be determined as the τ-axis intercept of the autocorrelation function (Poon et al. 1992) or the distance where the autocorrelation function becomes less than 10% (Thomas 1981).

However, the autocorrelation function is not without drawbacks. Profiles with a non-stationary mean, which is to say a profile that has a trend or recurrent structure, would not be properly described by the autocorrelation function (Sayles and Thomas 1977). Also, the correlation length is sensitive to filtering of the profile, particularly in regards to long wavelengths (Thomas 1981).

To address the autocorrelation function's disadvantages, Sayles and Thomas (1977) propose the structure function as an alternative since it can better show the effects of non-stationarity and easily detect filtering on the profile

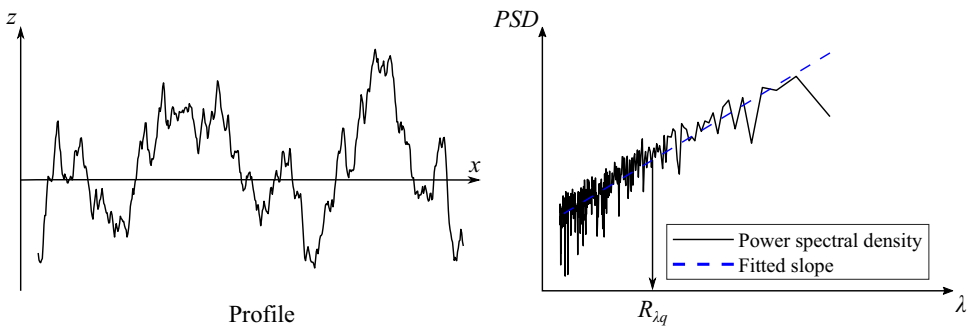

Fig. 5 The average profile wavelength ($R_{\lambda q}$) relates to the PSD function as a descriptor of the scale of observation (modified from Spragg and Whitehouse 1972)

since it is insensitive to the actual mean line of the profile. However, Bhushan (2000) argues that the structure function provides no more information than the autocorrelation function. This is immediately apparent when observing the relationships between the equations

$$\mathrm{SF}(\tau) = \lim_{L\to\infty} \frac{1}{L} \int_{L} [z(x) - z(x+\tau)]^2 \mathrm{d}x = 2R_q^2[1 - \mathrm{ACF}(\tau)] \tag{14}$$

since the structure function is simply an algebraic transformation of the autocorrelation function involving the RMS amplitude (R_q) (Bhushan 2000).

Nonetheless, the structure function can be used to relate to the JRC by substituting the lag distance, τ, with the profile sampling interval, creating a single parameter (Tse and Cruden 1979). This relationship has a strong quantitative correlation with the JRC, proving its capability in estimating peak shear strength (Tse and Cruden 1979; Yu and Vayssade 1991; Jang et al. 2014). However, Yu and Vayssade (1991) cautions that this relationship is very sensitive to the sampling interval. In their regression analysis, differences between regression parameters for different sampling intervals was very high indicating that small differences in the sampling interval could result in large variations in the calculated JRC.

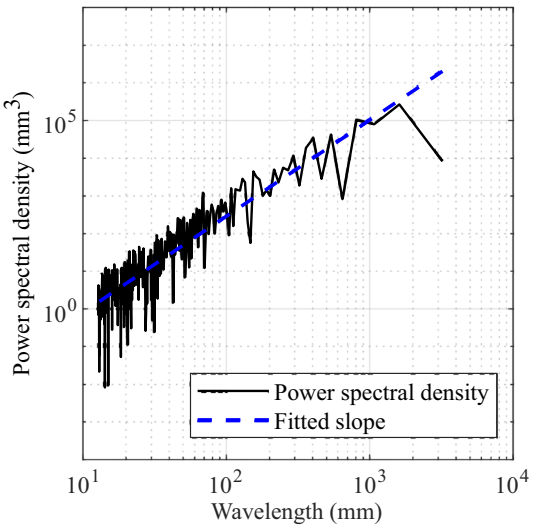

Fig. 6 An example of the PSD of a profile shown as the solid line with increasing wavelength. It should be noted that the synthetic profile was generated using the inverse Fourier transform and this representation may lack features that are not captured by the PSD. The dashed line is logarithmic linear regression that is further discussed as the PSD fractal characterization

2.2.2 Power Spectral Density

The power spectral density (PSD), denoted by $G(f)$, can be used to describe the magnitudes of waves of different wavelengths that compose a signal or profile; this can distinguish the relative significance of waviness and unevenness (i.e., long and short wavelength roughness, respectively). The PSD can be obtained by applying the Fourier transform to the autocorrelation function (ACF) as

$$G(f) = \frac{1}{L} \int_{-\infty}^{\infty} \mathrm{ACF}(\tau) \mathrm{e}^{-\mathrm{i}2\pi f\tau} \mathrm{d}\tau, \tag{15}$$

where f represents the frequency of a wave as a component of the autocorrelation function (Fig. 6) and i denotes an imaginary number. The wavelength ranges between the sampling frequency and the length of the sample (Power and Tullis 1991).

The PSD relates to the RMS roughness parameter, R_q, through

$$R_q^2 = \int_{\omega_0}^{\infty} G(f) \mathrm{d}f, \tag{16}$$

where ω_0 is the high cut-off frequency of the power spectrum (Sayles and Thomas 1978). Because of its relationship with R_q, the PSD demonstrates a greater degree of roughness characterization apart from profile variance. As with the ACF characterizations, the PSD is affected by sample non-stationarity, making challenging to capture and detect large wavelength characteristics (Dight and Chiu 1981). However, longer wavelengths have a greater effect on roughness compared to shorter wavelengths (Sayles and Thomas 1978). This makes the scaling of roughness parameters important to consider in surface roughness characterization.

The utility of the PSD is extended through the characterization of roughness as fractals which describe the scale-dependency of rough surfaces. This produces a linear trend in a log–log PSD plot (Fig. 6) as the Fourier transform naturally deconstructs profiles into wavelengths ranging between the sample length and the measurement resolution. Fractal characterization using the PSD is further discussed along with several other fractal estimation methods in the next section.

The evolution of rough surfaces that undergo shear displacement or wear can be characterized through the comparison of the PSD before and after their deformation (Whitehouse 1997). Power et al. (1988) compared the PSD spectra of a ground surface and a newly fractured surface of a granite laboratory sample. Both PSDs exhibited the same slope at short wavelengths, but the ground surface started decreasing in slope and plateauing at larger wavelengths.

They suggested that the decrease in slope was due to the grit size used (within range of the slope decrease) and the plateau is indicative of the flatness of the surface. As another example, PSD analysis revealed that earthquakes nucleation, growth, and termination on evolved faults are fundamentally different than on new ones (Sagy et al. 2007).

3 Fractal Characterization

Fractal mathematics were developed to describe phenomena that are seemingly random and are difficult to describe using Euclidean geometry. They are described as objects having a similar or identical pattern when observed at different scales (Mandelbrot 1967, 1982). In applying this to describing fracture roughness, studies found that surfaces exhibit self-affine fractal properties (Brown 1987; Power and Tullis 1991; Kulatilake et al. 1995; Renard et al. 2006; Tatone 2009). This contrasts from the more general class of fractal objects, self-similar fractals, in that self-affine fractals have different scaling values along the vertical and horizontal reference axes, whereas self-similar fractals scale isotropically (Power and Tullis 1991). This has implications on the methods used to analyze the rough surfaces since those based on self-similar fractals do not necessarily apply to self-affine fractals (Mandelbrot 1985; Kulatilake and Um 1999).

This scaling behavior is described as a power law observed as a line in logarithmic space in both the horizontal and vertical axes. The slope of this line is either directly or indirectly related to the fractal dimension, D, which can be used to describe the fractal's complexity (Malinverno 1990; Power and Tullis 1991). The Hurst exponent, H (named for the work done by Hurst (1951)), is directly related to D as $H = E - D$, where E is the number of spatial dimensions in which the fractal is measured (i.e., 2 for profiles, 3 for surfaces). D values for rock discontinuities typically range between 1 and 1.5 for profiles (possible range of 1–2) and 2–2.5 for surfaces (possible range of 2–3) (Brown 1987). This agrees with the definition of self-affine fractals where $D = 1.5$ for profiles compared to the self-similar definition where $D = 2$ (Brown 1987). The H value is more fundamental in describing fractals (Gallant et al. 1994). However, D and H are used interchangeably in literature (Brown 1987, 1995; Barnsley et al. 1988; Malinverno 1990; Odling 1994).

Several methods have been proposed to determine the D value of surfaces but with sometimes conflicting results (Kulatilake et al. 1995). This can be attributed to inaccurate surface measurement or errors in applying fractal concepts (Kulatilake et al. 1995; Tatone 2009). Kulatilake and Um (1999) also suggest that the amplitude parameter, which is the coefficient of the fractal power law relationship, is necessary to characterize roughness as a fractal.

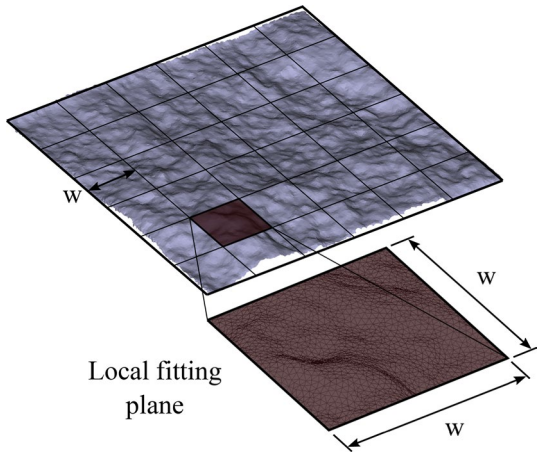

Fig. 7 Roughness-length method. Window subdivision on rock surface is carried out with square windows that are afterwards fitted to the points within the local fitting plane (modified from Fardin et al. 2001)

In this work, we focus our discussion on those methods that have been proven for the quantification of rough surfaces: the roughness-length method (Malinverno 1990), the PSD method, and the root-mean-square correlation function (Renard et al. 2006; Candela et al. 2009). These methods approach the characterization of roughness through different principles and have their own advantages and drawbacks. A number of other fractal methods that can potentially characterize rock roughness exist (Odling 1994; Kulatilake et al. 1998; Candela et al. 2009; Ge et al. 2014; Ban et al. 2018) but are not discussed here.

3.1 Roughness-Length Method

The roughness-length method calculates a standard deviation within local fitting lines or planes with respect to a "window", defining local areas for best-fit planes. The method was originally applied to 2D profiles (Malinverno 1990; Kulatilake and Um 1999) but was easily adapted for 3D surfaces (Lanaro 2000; Fardin et al. 2001). The surface is first subdivided into "windows" with a pre-determined size appropriate for processing (Fig. 7). The standard deviation relative to the local best-fit plane within each window is determined. A log–log plot relating the standard deviation and the window size is produced by varying window sizes and calculating the mean for each. This relationship is defined as

$$S(w) = \mathrm{RMS}(w) = \frac{1}{n_w}\sum_{i=1}^{n_w}\sqrt{\frac{1}{m_i - 2}\sum_{j\in w_j}\left(z_j - \bar{z}\right)^2}, \qquad (17)$$

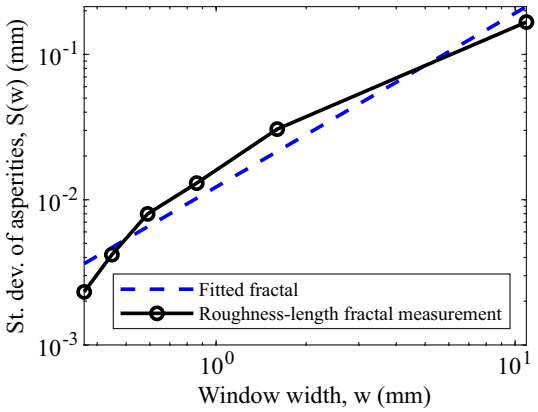

Fig. 8 Fractal dimension determination is conducted using log–log linear regression. The results for the queried window sizes are labeled with circles. The slope of the linear regression (in dashed lines) denotes the exponent and the intercept denotes the coefficient of Eq. (18)

where n_w is the number of windows, m_i is the number of points in the window, w_j is the jth window, and $z_j - \bar{z}$ is the difference between the measured surface points and the best-fit plane within window j (Fardin et al. 2001).

The fractal scaling behavior can be determined by applying a log–log linear regression to obtain fractal parameters from the equation

$$S(w) = Aw^H, \tag{18}$$

where w is the window width, $S(w)$ is the average standard deviation for a given window length, H is the Hurst exponent, and A is a proportionality constant (Fardin et al. 2001) (Fig. 8). While H is often expressed as a measure of roughness, A is also a measure of roughness amplitude dependent on the scale of roughness being studied (Kulatilake and Um 1999) and is similar to the statistical amplitude measured using R_q and R_a. While the windows used in this method are meant to be square, it has been suggested that anisotropic evaluation can be carried out with rectangular windows (Lanaro 2000).

Lanaro (2000) found that there is a window size above which rock surfaces can no longer be described as a fractal but instead as a stationary random process; this window size is called the stationarity threshold. This was determined by finding the window size at which $S(w)$ became constant. However, Fardin et al. (2001) suggest that the point where the fractal parameters, A and D, become constant with increasing sample size provides a more reliable way to establish the stationarity threshold. Furthermore, due to their constancy above the stationarity threshold, A and D are potentially able to describe rock roughness. Based on this observation, Fardin (2008) suggests that rock samples of sizes below the stationarity threshold are unable to fully characterize rock roughness and samples should be greater than this threshold to fully characterize field-scale roughness.

Fardin et al. (2001) suggest that the roughness-length method holds the advantage in removing the global trend of the entire rock surface. However, the choice of deciding where the windows should be located may be subjective and can change significantly the results if there are any significant departures from the regression plane.

3.2 Power Spectral Density

The PSDs of rock surfaces commonly feature a linear trend when plotted on a log–log graph. Brown and Scholz (1985) refer to this pattern as "red noise" since longer "red" wavelengths dominate in the PSD function. This slope can be modeled as a fractal relationship

$$G(f) = Cf^{-\beta}, \tag{19}$$

where C is an amplitude parameter, f is the dependent variable of the fractal representing the waves that compose the profile autocorrelation function, and β is the spectral exponent that is related to the Hurst exponent as $\beta = 2H + 1$ (Berry and Lewis 1980; Power and Tullis 1991; Gallant et al. 1994). The value β usually ranges between $2 < \beta < 3$ (Brown 1987). However, this relationship was contested and a different relationship $D \cong \frac{\beta}{2} + 2$ was proposed, implying that $H \cong \frac{\beta}{2}$ in consideration of a profile fractal, and is supported by results from Power and Tullis (1991). For rough surfaces, C describes the steepness of the surface topography while β describes the change with scale.

Another parameter called the "crossover length" defines a particular property characterized by the sample length being equal to the standard deviation (Wong 1987) and obtained when the PSD is transformed into

$$\int_f G(f)\mathrm{d}f = R_q = \sigma(\lambda_0) = b\left(\frac{\lambda_0}{b}\right)^{2-D}, \tag{20}$$

where b is the crossover length, λ_0 corresponds to the largest wavelength, and D is the fractal dimension. The σ refers to the standard deviation function of the profile with respect to λ_0. Here, we see again the relationship with RMS roughness parameter, R_q, which was already discussed in the statistical context of the PSD. The crossover length is directly related to the "topothesy" (κ) defined by Sayles and Thomas (1978) which can normalize the PSD of surfaces at different scales along a common slope (Berry and Hannay 1978; Brown 1987). The form that topothesy takes is determined as

$$\left[\sigma(\lambda_0)\right]^2 = \kappa\lambda_0^{2(2-D)}, \tag{21}$$

where κ is topothesy. The crossover length and topothesy relationship can be expressed as

$$\kappa = b^{2D-2} \tag{22}$$

since both relate to the PSD (Brown 1987). Upon closer inspection of these equations, we observe that the RMS roughness parameter, R_q, is dependent on the sample length scale, and that topothesy and crossover length are measures of the sample scale.

Candela et al. (2009) demonstrates the utility of the PSD in the determination of the Hurst exponent by comparison to different methods of estimation. Their findings show that the PSD does not exhibit any decrease of the H when comparing weathered and unweathered surfaces on the same fault. However, they successfully capture anisotropy and match the Hurst exponent determination over different scales.

3.3 Root-Mean-Square Correlation Function

Renard et al. (2006) evaluate the anisotropy of roughness for a strike–slip fault by determining the fractal characteristics for the relationship between the RMS of profile height difference and the length-wise interval used to obtain height differences. They establish the fractal relationship as

$$\sigma(\Delta x) = \alpha(\Delta x)^H, \tag{23}$$

where α is a fitting parameter, Δx is the interval for height difference, H is the Hurst exponent and $\sigma(\Delta x)$ is the RMS of the height difference calculated as

$$\sigma(\Delta x) = \sqrt{\frac{1}{N}\sum_{L} |z(x) - z(x + \Delta x)|^2}, \tag{24}$$

which is essentially the standard deviation of the absolute height difference along the profile.

This method was used to characterize fault surface roughness anisotropy through comparisons with the Hurst exponent evaluated using profiles captured along and perpendicular to the slip direction. Renard et al. (2006) use this method to characterize fault surface roughness anisotropy through comparisons with the Hurst exponent evaluated using profiles captured along and perpendicular to the slip direction. Candela et al. (2009) report similar results where RMS correlation function is able to exhibit anisotropic roughness with respect to the slip surface in comparison with other fractal evaluation methods they utilized in their study. They find that slip direction can be identified from directional RMS correlation function roughness, and that changes in H obtained through RMS correlation function effectively capture the weathering processes of surfaces exposed to climate. This difference with respect to the PSD method discussed in Sect. 3.2 (analyzing the same dataset yet unable to distinguish between weathered and unexposed surfaces) is attributed to the RMS correlation function method amplifying short wavelength features caused by weathering (e.g., pitting) (Candela et al. 2009).

4 Directional Characterization

Roughness characterization is recommended to be conducted along the direction of slip whether it is known or estimated (ISRM 1978). However, the process to capture geometric anisotropy has been relatively limited to evaluation of profiles set along different directions. For example, the PSD of profiles extracted parallel and perpendicular to fault slip has been of use to geophysicists in understanding faulting mechanisms (Power and Tullis 1991). RMS correlation function has also been proven to characterize anisotropy in exposed fault structures although this also required the use of parallel profiles obtained along chosen directions (Renard et al. 2006; Candela et al. 2009).

The directional roughness metric method directly links the analysis direction (i.e., direction of interest) with the roughness and its shear response without requiring the extraction of profiles (Grasselli et al. 2002; Grasselli and Egger 2003; Tatone and Grasselli 2009). Shear resistance increases based on the relative area of steeply sloped contact

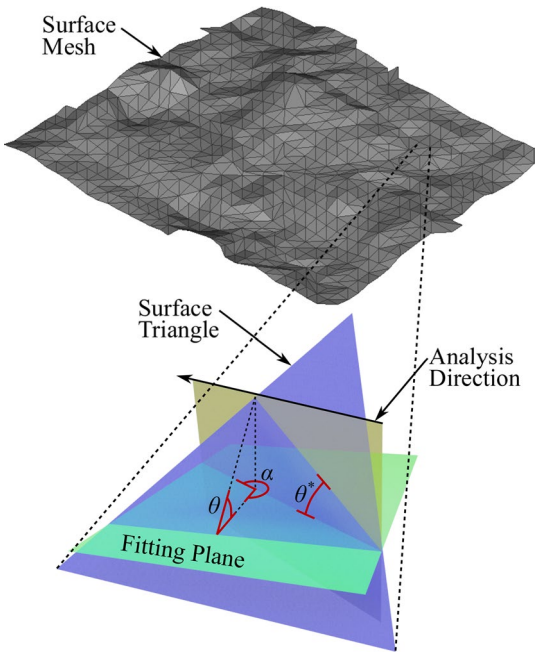

Fig. 9 Surfaces are constructed using triangles which have an absolute dip direction referred to as "true dip", θ. When analyzing roughness along a given analysis direction (α), each shear-facing triangle produces "apparent dip", θ^*, that is obtained as a relationship with θ and α according to Eq. (26). Each triangle's θ^* is then used to construct the cumulative distribution (after Tatone and Grasselli 2009)

points found on a surface. The slopes and distribution of these contacts change depending on the analysis direction which changes the transmission of forces across the joint. This implies that only the potential contact areas should be considered in the evaluation of roughness influencing shear strength of rough joints (Grasselli et al. 2002). The core of this idea is similar to the Z_2 statistical parameter where the slope of the function is directly measured from a profile. However, the directional roughness metric encompasses a three-dimensional approach with greater consideration to the potential contact areas. Z_2 is also not selective of shearing direction.

The analysis method begins with the surface being reconstructed from point elevation measurements as a triangular polygon mesh. Triangles facing against the analysis direction are kept for analysis while the other triangles are filtered out since only the fraction of the surface facing against the analysis direction can provide shear resistance. The strike and dip concepts used in structural geology are used to describe each triangle's influence on roughness. An apparent dip is determined based on a triangle's normal vector in relation to the analysis direction. These are related as

$$\tan\theta^* = -\tan\theta\cos\alpha, \tag{25}$$

where θ^* is the apparent dip angle, θ is the true dip of the triangle, and α is the angle between the normal vector azimuth and the analysis direction (Grasselli et al. 2002) (Fig. 9). A decreasing cumulative area fraction distribution with respect to θ^* is obtained by summing the triangular area fraction with an apparent dip greater than θ^* for each queried θ^* (Fig. 10). This provides a power distribution fitted as

$$A_{\theta^*} = A_0\left(\frac{\theta^*_{\max} - \theta^*}{\theta^*_{\max}}\right)^C, \tag{26}$$

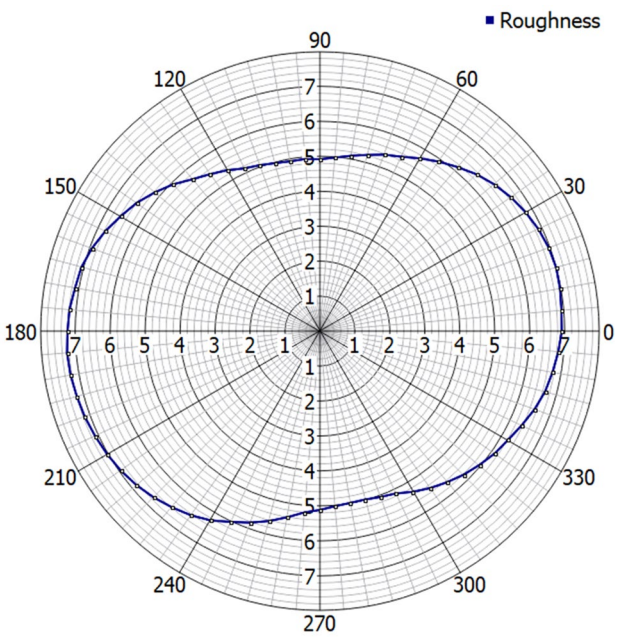

Fig. 11 Directional roughness metric plotted radially along the rock surface based on the direction along which roughness is calculated. The line corresponds to roughness and expresses the parameter $A_0\theta^*_{\max}/(C+1)$

where A_0 is the normalized cumulative area of all polygons facing the analysis direction, $\theta^*_{\max}$ is the maximum measured apparent dip angle, and C is the fitting parameter. The fitting parameter, C, must be determined using a non-linear regression method since the log–log transformation of this equation results in a non-linear relationship. By obtaining these parameters based on a shearing direction, roughness anisotropy can be clearly observed (Tatone and Grasselli 2009).

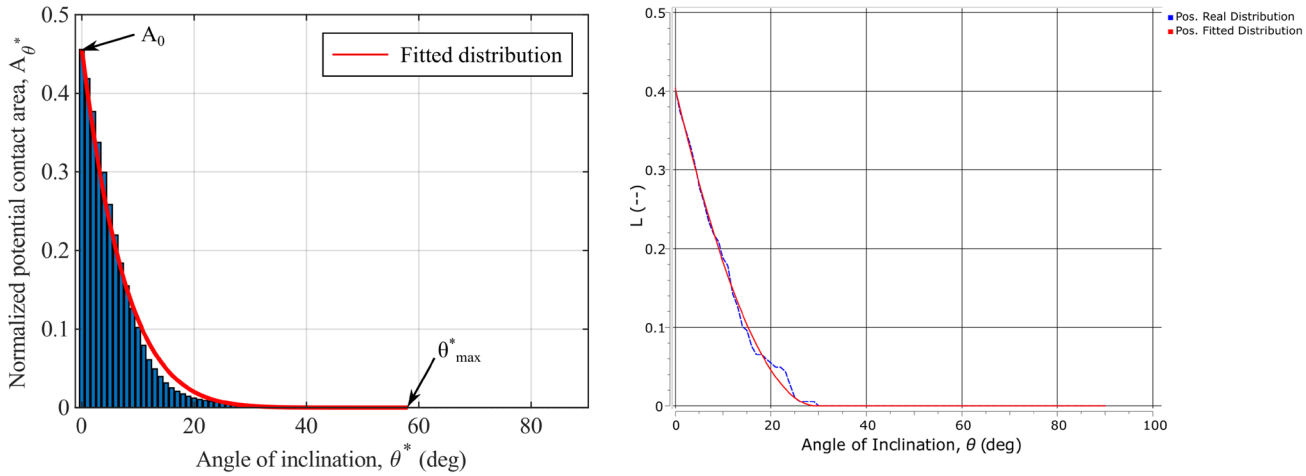

Fig. 10 The cumulative distribution of potential contact area, A_{θ^*}, with respect to apparent dip, θ^*, and showing the fitted distribution, C

After determining the fitting parameter, C, the maximum apparent dip angle, θ^*, and the normalized potential contact area, A_{θ^*}, for every given analysis direction, a radial plot can be created to describe directional roughness (Fig. 11). The parameter $\theta^*_{\max}/C$ was originally proposed by Grasselli et al. (2002) which has been shown to qualitatively reflect roughness anisotropy. However, Tatone and Grasselli (2009) found that the area under the fitted distribution curve, calculated as $A_0\theta^*_{\max}/(C+1)$, better describes roughness anisotropy since it considers the total potential contact area, the concavity of the fitting curve, and the steepest apparent dip experienced along the analysis direction. The parameter $A_0\theta^*_{\max}/(C+1)$ carries a more rigorous mathematical explanation by considering the area under the fitting curve with a range of $C \in [0, \infty)$ and avoids excessively large values as $C \to 0$. The parameter A_0 provides a measure of the contact area but tends to vary slightly around the value 0.5 and may not carry much significance in characterizing directional roughness (Tatone and Grasselli 2009; Liu et al. 2017; Tian et al. 2018). However, in cases of significant differences of A_0 along different directions (e.g., ripples), the roughness parameter can be described as $2A_0\theta^*_{\max}/(C+1)$ to be comparable with the simplified case of $A_0 = 0.5$ that produces the parameter $\theta^*_{\max}/(C+1)$.

The parameter $\theta^*_{\max}$ tends to vary significantly with considerable dependency on the measurement resolution as it was observed that this parameter tends to approach 90° with increasing measurement resolution. Also, large variations of $\theta^*_{\max}$ have been measured from samples created as replicas of the same fracture surface (Tatone 2009; Tian et al. 2018) showing unreliability in using this parameter. With this considered, Tian et al. (2018) propose that $\theta^*_{\max}$ can be fixed as 90° and resultant fitting parameter denoted as C'. The reasoning for this adjustment is that with increasing resolution eventually a 90° angle would be observed whereas C is a more consistent parameter. Their study found little difference between the original parameter by Tatone and Grasselli (2009) and the modified directional roughness metric $90°/(C'+1)$, implying that $\theta^*_{\max}$ is not significant in the estimation of roughness. For ideal situations where the fitting curve follows a power distribution closely and the actual $\theta^*_{\max}$ is sufficiently high enough, this assumption in calculating C' may be reasonable.

5 Discussion

5.1 Applications

The mechanical and fluid flow properties of a fracture are highly dependent on the surface roughness. It is known that contacting matched surfaces only connect at portions of the total surface (Dieterich and Kilgore 1994; Grasselli et al. 2002; Zhao et al. 2018). This complicates mechanical property estimation in addition to the challenges already associated with roughness characterization. However, roughness characterization and the mechanics of surface interaction have been demonstrated to exhibit empirical correlation (Tse and Cruden 1979; Brown and Scholz 1986; Maerz et al. 1990; Yu and Vayssade 1991; Olsson and Brown 1993; Yang et al. 2001; Tatone and Grasselli 2010; Jang et al. 2014). Thus, making correlations between roughness parameters and shear strength and aperture help reframe the variability of roughness into parameters suitable to estimate mechanical and hydromechanical behavior for rough interfaces.

5.1.1 Shear Strength Evaluation

Prediction of shear strength of rock joints accounting for roughness was pioneered by Barton (1973) through empirical relationships involving the JRC, which was back-calculated from direct shear test results. Example profiles exhibiting a range of JRC were later established by Barton and Choubey (1977). This relationship was implemented in determining the slope of the Mohr–Coulomb failure criterion using the equation

$$\tau = \sigma_n \tan\left(\mathrm{JRC} \times \log\left(\frac{\mathrm{JCS}}{\sigma_n}\right) + \varphi_r\right), \tag{27}$$

where the JRC is implemented in the friction angle term sensitive to the joint wall compressive strength parameter (JCS) and the normal stress (σ_n). The parameter φ_r is defined as the residual friction angle meant to represent the shear strength after exceeding peak strength. Example profiles representing a range of JRC values empirically correlating roughness with the peak shear strength envelope was published by Barton and Choubey (1977). However, usage of these profiles to evaluate JRC is a qualitative and subjective procedure with significant variance observed between practitioners (Beer et al. 2002). This implies that JRC-related methods cannot be efficiently accounted for in design standards and highlights the need for an objective measure of roughness. To introduce objectivity in estimating JRC, correlations against roughness parameters determined from digitized JRC profiles were proposed with relatively successful results (Tse and Cruden 1979; Maerz et al. 1990; Yu and Vayssade 1991; Yang et al. 2001; Tatone and Grasselli 2010; Jang et al. 2014).

Most roughness parameters used in estimating the JRC for shear strength do not explicitly consider directionality of roughness (i.e., roughness anisotropy) (Liu et al. 2018) and include parts of surfaces that theoretically should not contribute to shear strength with certain directions (leeward side of asperities). Tatone and Grasselli (2010) adapted the directional roughness metric $\theta^*_{\max}/(C+1)$ for use in 2D profiles by simply obtaining the cumulative length distribution of increasing θ^* values in the analysis direction. This metric was correlated with digitized and modified JRC profiles

derived from Barton and Choubey (1977) and provided fairly agreeable results. Anisotropy was observed since the directional roughness metric going both forwards and backwards in the same profile was different. This added to the variability in correlating $\theta^*_{\max}/(C+1)_{2D}$ to the JRC. To correlate the JRC with the directional roughness metric, the average of the forward and backward metric was used. Anisotropy is expected as the direction of shear when selecting these profiles was not explicit or considered in Barton and Choubey (1977).

The peak shear strength criterion introduced by Grasselli and Egger (2003) and further updated by Cottrell (2009, as cited by Tatone et al. 2010) directly implements the directional roughness parameter in shear strength prediction as

$$\tau = \left[1 + e^{-\frac{\theta^*_{\max}}{C+1} \times \frac{\sigma_n}{9A_0\sigma_t}}\right] \sigma_n \tan\left[\varphi_b + \left(\frac{\theta^*_{\max}}{C+1}\right)^B\right], \tag{28}$$

where σ_n is the normal stress applied, σ_t is the tensile strength of the material, φ_b is the basic friction angle, B is an empirical fitting parameter, A_0 is the normalized total potential contact area, and $\theta^*_{\max}/(C+1)$ is the directional roughness metric. The fitting parameter B is sensitive to the resolution of the mesh and the length of the sample. This fitting parameter is discussed along with the effects of resolution on shear strength in Sect. 5.3.

Further modification on the peak shear strength criterion by Grasselli and Egger (2003) was done while retaining the roughness parameters A_0, C, $\theta^*_{\max}$ (and subsequent modifications to these parameters) to expand the range of applicability to areas where Eq. (28) does not apply. These have typically taken the form

$$\tau = \sigma_n \tan\left(\varphi_b + \varphi_{sr}\right), \tag{29}$$

where φ_{sr} is referred to as the roughness contribution angle that is the subject of proposed modification. This form deviates from Eq. (28) by removing the maximum peak friction angle term, $\left[1 + \exp\left(-\frac{\theta^*_{\max}}{C+1}\frac{\sigma_n}{9A_0\sigma_t}\right)\right]$. φ_{sr} is used here as a catch-all term for surface roughness since the modifications made to the peak shear strength criterion in each study consider different mechanisms for the shear strength contribution of roughness.

Xia et al. (2014) suggested a peak dilatancy angle function, i_p, as the sole contributor of roughness to shear strength as

$$\varphi_{sr} = i_p = \frac{4A_0\theta^*_{\max}}{C+1}\left[1 + \exp\left(-\frac{1}{9A_0} \times \frac{\theta^*_{\max}}{C+1} \times \frac{\sigma_n}{\sigma_t}\right)\right]. \tag{30}$$

Tang and Wong (2016) expanded on Eq. (30) by applying a "joint contact state coefficient", JCC, that considers the matching between both sides of a joint as

$$\varphi_{sr} = \mathrm{JCC} \times i_p = \left[\frac{1}{\left[1 + 8A_0\theta^*_{\max}/(C+1)\right] \times \kappa}\right] \times \frac{4A_0\theta^*_{\max}}{C+1}\left[1 + \exp\left(-\frac{1}{9A_0} \times \frac{\theta^*_{\max}}{C+1} \times \frac{\sigma_n}{\sigma_t}\right)\right], \tag{31}$$

where $\kappa = d/l$, or the ratio of the displacement between two matching surfaces (d) to the length of the sample (l). Yang et al. (2016) proposed a joint effective asperity angle, α_e,that both considers the asperity angle and the JCS term used in Eq. (29) as

$$\varphi_{sr} = \alpha_e = \frac{\theta^*_{\max}}{C^{0.45}} \exp\left(-\frac{\sigma_n}{\mathrm{JCS}} C^{0.75}\right). \tag{32}$$

Liu et al. (2018) use a modified apparent dip distribution fitting considering the ratio of the initial contact area to the total potential contact area. While this fitting is similar to the directional roughness metric method discussed in Sect. 4, it instead produces a characteristic angle, $\overline{\theta^*}$, and a parameter representing the distribution, n. These parameters are used along with the average surface height from the fitting plane to obtain a peak dilatancy angle that tends to 0 as $\sigma_n \to \infty$. These parameters are implemented as a peak dilatancy angle which is used in Eq. (29) as

$$\varphi_{sr} = i_p = \left(\frac{\overline{\theta^*}}{n}\right)^{0.88} \times h \times \exp\left(-\frac{\sigma_n}{\sigma_c} \times h^2\right), \tag{33}$$

where σ_c is the unconfined compressive strength in MPa and h is the average joint height in mm with respect to the best-fit plane. The method to determine h is the 3D equivalent to R_a determined using Eq. (1). Tian et al. (2018) also propose a modification to the directional roughness metric parameters as mentioned in Sect. 4. This produces a peak shear strength criterion using C' as the sole roughness parameter along with normal stress and tensile strength in determining the peak dilation angle as

$$\varphi_{sr} = i_p = \frac{160 \times C'^{-0.44}}{\sigma_n/\sigma_t + 2}. \tag{34}$$

5.1.2 Aperture Evaluation

When two rough surfaces are placed against each other, void space will always exist between them regardless of their matching. This effect is often due to degree of mismatching of asperities that can exist at any scale dimension. When describing rock mass discontinuities, the space between two interacting surfaces is referred to as "aperture" (ISRM 1978). In rock masses, discontinuity apertures are capable of transporting fluids much faster than intact rock. While knowing the aperture may help understand fluid flow,

its estimation is made difficult with stresses and resultant displacements acting on the discontinuity since they are affected by surface roughness. Since this creates complexity on the fluid dynamics occurring in a rough fracture, aperture effects on fluid flow can be simplified as two parallel plates. This concept is used in the cubic flow law which states that the laminar flow rate between two parallel plates is proportional to the cube of the aperture (Zimmerman and Bodvarsson 1996). This is typically valid for closed fractures under high normal stress (Witherspoon et al. 1980); however, variations in aperture and turbulent flow due to roughness can cause significant deviation from the cubic flow law (Zimmerman and Bodvarsson 1996). Although this has provided a useful approximation, modern evaluation of fluid flow through joint apertures is possible using digitized surfaces from computed tomography scanning (Crandall et al. 2010; Jing et al. 2017) and direct surface scanning (Tatone and Grasselli 2012; Busse et al. 2015; McCraw et al. 2016) in fluid dynamics simulations.

The effects of stresses on aperture are measurable but require consideration of the roughness of the contacting surfaces. As previously mentioned, fractured rock surfaces do not perfectly match when aligned back together as evidenced by contact area (Dieterich and Kilgore 1994; Zhao et al. 2018) and aperture studies (Yeo et al. 1998). The imperfect contact affects the way that normal stress, shear stress, shear displacement, and roughness geometry are interrelated. For example, shear displacement of a rough surface causes dilation which can affect its normal stress given displacement constraints along the normal direction. Another example is when roughness affects the contact area on which normal force is applied and can change the stiffness of rock across a joint (Raven and Gale 1985; Olsson and Brown 1993).

Roughness characterization has typically been used to either observe the mechanical and geometric effects to which aperture is sensitive or to directly account for those effects to explain deviations from the cubic flow law. When applying roughness characterization to a fracture, the combined effects of the two surfaces are analyzed by obtaining the difference between the surface heights. The resultant difference, which is essentially the aperture distribution, can be analyzed as a composite surface as it contains information from both surfaces of the fracture (Brown 1995; Matsuki et al. 2006). As the simplest of roughness characterization methods, statistical concepts can be easily applied to analyze the variation of aperture. Brown and Scholz (1986) demonstrated its potential use by fitting a negative exponential distribution on the upper tail of the aperture distribution for varying normal stress states to predict aperture closure. However, Olsson and Brown (1993) found that the predicted stiffness was higher than expected when the surfaces were matched at zero shear displacement yet agreed more closely with laboratory results when surfaces were displaced. This relationship is likely to be scale dependent as Koyama et al. (2006) found that the mean and standard deviations of aperture increase with sample size.

Functional roughness characterization methods, including the PSD, variogram analysis, fractal characterization, and the aperture density distribution, have also been broadly used to characterize aperture. Brown et al. (1986) found that the PSD aperture distribution profile plateaus at lower frequencies compared to the surface profile PSD. This causes the R_q value of the aperture profile to plateau even as the profile length increases. The corresponding wavelength at which this change occurs is called the "correlation distance", representing the length above which two surfaces can be considered as "matched" (Brown and Scholz 1985). These are similar to the "mismatch length" discussed by Olsson and Brown (1993). Lanaro (2000) equated this to the stationarity threshold as the plateau in fractal parameters is closely related to the plateau found in the aperture PSD where wavelengths above the correlation distance no longer match between each other. Brown et al. (1986) also used a frequency-dependent aperture/surface PSD ratio

$$R(f) = \frac{\text{aperture PSD}}{\text{surface PSD}} = \frac{G_{\text{aperture}}(f)}{G_{\text{surface}}(f)}, \tag{35}$$

to understand the relationship between the surfaces and their corresponding aperture. They show that $R(f)$ is equal to 2 when approaching higher frequencies. This implies that the two surfaces become uncorrelated and independent at higher frequencies. As the variance of the sum of two independent random functions is equal to the sum of the respective variances of these functions, the aperture PSD would show twice the variance of the surface PSD when they become uncorrelated (Brown et al. 1986). A semivariogram analysis by Yeo et al. (1998) was done to compare the differences in correlation of the aperture distribution with respect to the shearing direction. The aperture was more closely correlated perpendicular to shear compared against parallel to shear.

5.1.3 Synthetic Roughness

When obtaining quantitative measures describing surface roughness, the question may arise whether the relationship between the data and the result is bidirectional or if there exists no inverse operation. Brown (1995) describes a methodology modified from Barnsley et al. (1988) to create an anisotropic surface and aperture by applying the inverse Fast Fourier Transform with the PSD. A surface generation program is used to create an initial surface and an aperture distribution. Using the power law relationship (Eq. 19), the PSD can be estimated if the proportionality constant (C) and exponent (β) are known. R_q can be used to approximate C through Eq. (16) due to its relationship with height variance.

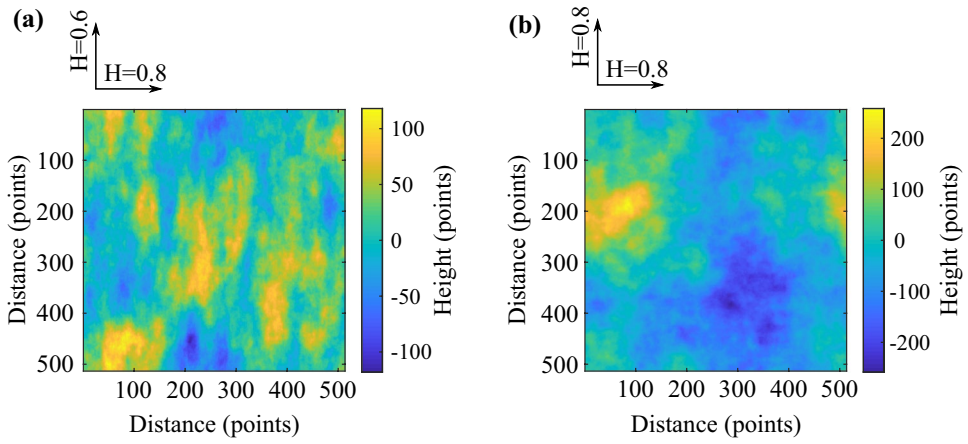

Fig. 12 Synthetic surface roughness can be produced with **a** anisotropic roughness and **b** isotropic roughness (after Candela et al. 2009)

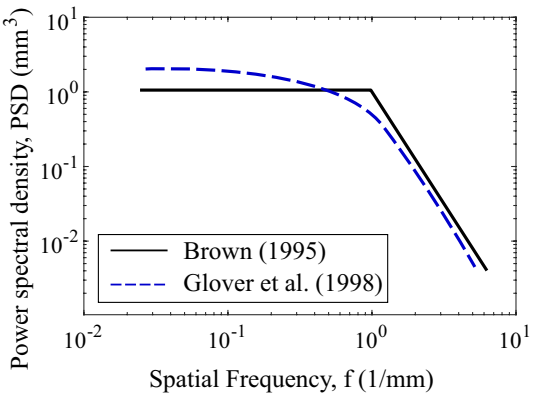

Fig. 13 PSD comparison showing the synthetic aperture generation methods suggested by Brown (1995) (solid) and by Glover et al. (1998) (dashed). A threshold for the PSD exists at the mismatch length frequency (where the discontinuity occurs) for aperture synthesis

Similarly, β can be estimated through the fractal dimension, $D = (7 - \beta)/2$ or the Hurst exponent, H. Brown (1995) considers these two parameters to be sufficient in generating realistic surfaces.

The algorithm begins by defining complex number amplitude spectrum using polar coordinates. Random number generators providing uniformly distributed numbers between 0 and 2π are used in defining the phase coordinate while the radial coordinate (r) follows an equation derived from the PSD relationship as

$$r = \left(i^2 + \frac{j^2}{(\text{anisotropy factor})^2} \right)^{-\frac{H+1}{2}}, \tag{36}$$

where i and j relate to the spectral frequencies of the surface, the anisotropy factor controls the trend of the surface along the x and y coordinates, and H is the Hurst exponent related with the fractal dimension (D) and the spectral exponent (β).

Candela et al. (2009) provide a similar algorithm that also considers anisotropy (Fig. 12).

While surface generation is relatively straightforward, generation of the opposite surface for aperture requires closer attention. Brown (1995) originally conceptualizes the second surface to be generated with consideration to the "mismatch length scale". Two wavelengths are suggested by Brown (1995) for the mismatch length scale. The first estimate is the wavelength at which the ratio of the aperture-surface PSD ratio, $R(f)$, crosses unity and is denoted as $\lambda_c^{(1)}$. The second estimate of the mismatch length scale is made using $R(f) = 2$ and is denoted as $\lambda_c^{(2)}$. The opposite surface is generally correlated at larger wavelengths. However, this correlation ends when wavelengths shrink below the mismatch length scale. Brown (1995) demonstrates the expected aperture PSD when this correlation scheme is implemented, exhibiting a constant flat section at the larger correlated wavelengths (Fig. 13). This is achieved by using a second random number generator different from the one used for generating the initial surface, thus, decorrelating the two surfaces and creating the characteristic spectral slope. Amplitudes for wavelengths larger than the mismatch length scale are determined with the same random numbers used to generate the first surface.

However, Glover et al. (1998) argued that the correlation change relating to the mismatch length scale should not be a sharp discontinuity but rather a frequency-dependent gradation (Fig. 13). This would produce more realistic aperture PSD functions. The rate at which two surfaces match with respect to the frequency is governed by the weighting function, $\gamma(k)$,

$$\gamma(k) = \beta_{\text{roll-off}} \left(1 - \frac{k}{2k_c^{(2)}} \right), \tag{37}$$

where $\beta_{\text{roll-off}}$ is the roll-off parameter, k is the frequency (or wavenumber), and $k_c^{(2)}$ is the frequency (based on the corresponding wavelength $\lambda_c^{(2)}$). $\beta_{\text{roll-off}}$ adjusts the sharpness of the bend in the PSD and $k_c^{(2)}$ adjusts the mismatch length frequency. Glover et al. (1998) found that $k_c^{(2)}$ produces more realistic surfaces. The weighting function is implemented as

$$R_3 = R_1\gamma + R_2(1-\gamma), \tag{38}$$

where R_1 and R_2 are the random numbers generated independently for each surface. When generating the aperture, R_3 defines the random number used in determining the phase coordinate. This gradually increases the correlation between the two surfaces as the frequency decreases producing more realistic apertures. However, later work by Ogilvie et al. (2006) recognizes that algebraically combining sets of random numbers breaks down the uniform distribution produced by the random generators. Thus, they propose an algorithm gradually swapping numbers between these two sets with the goal of gradual correlation between the aperture and the initial surface as the wavelength increases.

Matsuki et al. (2006) extend the use of the aperture-surface ratio by fitting a curve along the $R(f)$ relationship to generate synthetic apertures larger than the measured sample through extrapolation. This assumes that a surface PSD will continue to follow a power law with increasing wavelength as the aperture approaches a limit. Although this approach may provide reasonable results, this relationship may be sensitive to the stationarity threshold which has been observed to affect the scaling behavior of rough surfaces (Lanaro 2000; Fardin et al. 2001, 2004; Fardin 2008).

5.2 Parameter Selection

In earlier times, it was understood that a single roughness characterization method alone is insufficient to fully characterize roughness (Spragg and Whitehouse 1970). However, depending on the application many parameters could be useful, while others may not. For example, the averaged height parameter, R_a, provides only relative height information and does not consider spatial characteristics such as the RMS slope parameter, Z_2. The statistical parameters standardized by the ISO had greater relevance to the machining industry as they provided a quick and easy quality control methodology when technology was not sufficiently advanced for more sophisticated calculations (Whitehouse 1994).

When using fractal characterization methods, the obtained values are sensitive to the method used in characterizing the fractal. The selected input parameters for each method and the accuracy of surface measurement can significantly impact the calculated fractal parameters. As a result, there has been some controversy surrounding the suitability of fractal approaches for quantifying discontinuity roughness. Some studies have shown different analysis methods to give conflicting values of D or the analysis method to give different results for the same surface when using different analysis input parameters (Tatone and Grasselli 2013).

Much of the other published conflicting results can be attributed to either poor measurement (i.e., high noise or coarse resolution) or erroneous analysis methods (i.e., application of self-similar analysis methods to self-affine profiles or unsuitable parameter selection for self-affine methods). To overcome these problems and achieve consistent estimates of self-affine fractal parameters, an attempt is made to create "suggested methods" for the variogram, spectral, and roughness-length methods to improve consistency in obtaining self-affine fractal parameters (Shirono and Kulatilake 1997; Kulatilake et al. 1998; Kulatilake and Um 1999).

Two-dimensional (2D) profiles are projections of the topographic elevation of three-dimensional surfaces captured by a given line on the surface. This process inherently masks some features that the surface may exhibit, of which, some may play an important role in roughness shear strength (Grasselli et al. 2002). The process of selecting 2D profiles may also introduce bias that may hide or exaggerate key roughness features (Tatone and Grasselli 2009). Consequently, a 3D roughness characterization method that can effectively integrate all features for surface roughness is required especially when shear strength must be estimated.

Surface measurement technologies have advanced to a state where detailed measurements can be taken almost instantaneously (Tatone and Grasselli 2009). A variety of surface measurement techniques have been employed including photogrammetry (El-Soudani 1978), fringe projection stereo-camera (Grasselli et al. 2002; Tatone 2009; Tatone and Grasselli 2009), laser slit scanning (Lanaro 2000), lidar (Fardin et al. 2004; Sagy et al. 2007), and laser autosynchronous triangulation scanning (Mah et al. 2013). Computing power has also improved allowing consumer-level computers to feasibly process data on such a scale. These factors allow for larger, high-resolution surface roughness analysis of rock surfaces. Thus, 3D roughness characterization methods should be considered, whenever possible, since they provide a more representative analysis of the surface characteristics and eliminate much of the bias inherent in the use of 2D surfaces (e.g., loss of significant asperities, relationship of features perpendicular to shear direction).

5.3 Measurement Resolution and Scaling

Rough surfaces exhibit different patterns in geometry with changing scale and can be described using self-affine fractal concepts (Brown 1987). A surface that may appear smooth to the naked eye, may be described as rough at microscopic scales. It would follow that, because of the scale-dependency of roughness, changing scale indirectly influences surface contact mechanics such as shear strength and dilation. This

is especially important as it highlights one of the major barriers in reconciling lab-scale testing and field-scale observations (Sayles and Thomas 1978; Brown and Scholz 1985; Renard et al. 2006; Sagy et al. 2007; Candela et al. 2009).

Tatone and Grasselli (2013) investigated the effects of resolution and scaling on roughness parameters done by previous work. In their review, it was suggested that the roughness is highly sensitive to the resolution of the profile or surface measurement. Variation in measurement resolution between the various studies may have skewed results from scaling studies causing the conflict between reported results. For example, Fardin et al. (2004) and Fardin (2008) find to have consistent surface scanning throughout the work completed within their respective studies. However, the results they produced conflicted (the former with negative scale effects and the latter with positive scale effects) since the earlier study had a lower resolution. This sensitivity to resolution complicates roughness analysis. As such, it is recommended that the measurement resolution must be reported and that the highest resolution possible is used to capture a greater amount of roughness features (Tatone and Grasselli 2013). This would also allow for the investigation of roughness at lower resolutions as the surface can be resampled at a later time if necessary.

Since the measured roughness can change significantly with resolution, these effects should be accounted for when estimating physical behavior. The effects of sampling are apparent in work by Yu and Vayssade (1991) where they determined empirical relationships between roughness parameters and the JRC that yielded equations strongly sensitive to the sample interval. Tatone et al. (2010) suggest accounting for resolution in the calibration of the B parameter of the equation suggested by Cottrell (2009) (Eq. 28), which is the exponent of the roughness parameter $\theta^*_{\max}/(C+1)$ within the friction angle term. A power relationship between B and the surface resolution of the form $B = a(r)^p$ can be made where r is the surface resolution while a and p are both fitting parameters. B for each surface resolution is determined from Eq. (28) using a single shear strength test and a series of surface meshes corresponding to r. This allows for the prediction of shear strength using the roughness parameter given an arbitrary measurement resolution. However, this relationship must be further studied as it was only verified for a single series of surface roughness replicas and the best possible resolution should still be used to capture as many roughness features as possible (Tatone et al. 2010; Cottrell et al. 2010).

6 Roughness Calculator Application

The analysis of roughness can be tedious and computationally intensive especially considering the importance of having higher quality resolution and larger sample sizes. To alleviate the time and effort put into the processing stage, a 2D and 3D roughness calculator was created as an open-source package by the authors implementing many of the methods discussed in this work. The package is available on the Geomechanics Group @ University of Toronto website (http://www.geogroup.utoronto.ca/?ddownload=5130). The Qt C++ framework (The Qt Company 2018) was used to develop the graphical user interface and the QwtPolar/Qwt libraries (Rathmann 2014; Rathmann and Wilgen 2016) were used for scientific plotting. Linear algebra operations were handled by the Armadillo Linear Algebra Library (Sanderson and Curtin 2016). This calculator accepts STL files for 3D surface processing and 2D CSV files for 2D profile processing. The spatial dimension is detected based on the type of file provided. The application is discussed in detail in Appendix 2.

7 Conclusions

Three distinct categories of methods are described in this work: statistical, fractal, and directional characterizations. Although we categorize these methods into the mentioned types, many were developed with similar ideas between these categories. Statistical characterization draws from the branch of mathematics mentioned in the name to constrain the apparent random nature of the surface into a form of structure. This category was further subdivided into parameter and functional characterization. Parameter characterization provides singular values that describe the general height or spatial trends of the surface. Functional approaches provide a visual structure to describe roughness with greater detail than single parameters, such as the PSD with its spectral description of different waves that comprise a rough surface.

The PSD also lends to fractal characterization which describes the relationship of roughness with different scales of observation. Rough surfaces are considered to be self-affine fractals which are described using a fractal dimension. However, there are many different methods that require deeper understanding of their individual approach. These differences in approach should be carefully considered when applying them to practice.

Directional characterization provides understanding of the anisotropy of roughness on surfaces. Early attempts to differentiate roughness anisotropy have amounted to simply orienting profiles along different directions of interest. However, this method of measurement potentially constrains localized features to few profiles when they may be critical to roughness characterization in all profiles. The directional roughness method presented in this work (Grasselli et al. 2002; Grasselli and Egger 2003; Tatone and Grasselli 2009) takes the entire surface into consideration with exclusion only to areas considered not in contact

when considering a hypothetical shear displacement on the surface. However, this method is sensitive to measurement capabilities and care should be taken to ensure the surface quality before undertaking analysis.

Roughness has been relatively difficult to quantify and is apparent in the multitude of methods proposed. However, because these methods share similar ideas, it is not necessarily difficult to understand the mechanisms of their characterization. There is great value in having quantitative measures of roughness that removes the dependence on subjective experience. The discussed roughness characterizations can be applied to shear strength prediction, aperture evaluation for fluid transmissivity analysis, and synthesis of virtual rough surfaces. Moreover, the authors provide an open-source program to process roughness surface data.

Acknowledgements This work has been supported through the NSERC Discovery Grants 341275, the NSERC CREATE ReDeveLoP program, and the NSERC/Energi Simulation Research Chair in "Fundamental rock physics and rock mechanics" program. The software developed in this study can be accessed from our data server (http://www.geogroup.utoronto.ca/?ddownload=5130).

Appendix 1

The formulas used and the works that they are derived from are listed below in Table 1.

Table 1 A summary of the roughness parameters and typical symbols seen in literature

Variable	Formula	Description	2D program	3D program	Sources
CLA, R_a	$\mathrm{CLA} = 1/L \int_{x=0}^{x=L} \lvert z \rvert \mathrm{d}x$	Average height from profile reference	Y	–	Whitehouse (1994) and ISO (1997)
RMS, Z_1, R_q	$\mathrm{RMS} = \sqrt{\frac{1}{L}\int_{x=0}^{x=L} z^2 \mathrm{d}x}$	Similar to CLA, variance of height	Y	–	Myers (1962) and Whitehouse (1994)
R_{sk}	$R_{\mathrm{sk}} = \frac{1}{R_q^3}\left(\frac{1}{L}\int_L z^3 \mathrm{d}x\right)$	Profile skewness	Y	–	Whitehouse (1994) and ISO (1997)
R_{ku}	$R_{\mathrm{ku}} = \frac{1}{R_q^4}\left(\frac{1}{L}\int_L z^4 \mathrm{d}x\right)$	Profile kurtosis	Y	–	Whitehouse (1994) and ISO (1997)
$Z_2, R_{\Delta q}$	$Z_2 = \sqrt{\frac{1}{L}\int_{x=0}^{x=L}\left(\frac{\mathrm{d}z}{\mathrm{d}x}\right)^2 \mathrm{d}x}$	RMS of profile slopes	Y	–	Myers (1962)
$Z_3, R'_{\Delta q}$	$Z_3 = \sqrt{\frac{1}{L}\int_{x=0}^{x=L}\left(\frac{\mathrm{d}^2z}{\mathrm{d}x^2}\right)^2 \mathrm{d}x}$	RMS of profile curvature	Y	–	Myers (1962)
A_{i}	$A_{\mathrm{i}} = \tan^{-1}\left(\frac{1}{L}\sum_{i=1}^{N-1}\lvert z_{i+1} - z_i \rvert\right)$	Average height increase angle	Y	–	Tatone (2009)
R_{p}	$R_{\mathrm{P}} = \frac{L_{\mathrm{t}}}{L_{\mathrm{n}}} = \frac{\sum_{i=1}^{N-1}\sqrt{(x_{i+1}-x_i)^2+(z_{i+1}-z_i)^2}}{L_{\mathrm{n}}}$	Ratio of true length over nominal length	Y	–	El-Soudani (1978)
R_{s}	$R_{\mathrm{S}} = \frac{A_{\mathrm{t}}}{A_{\mathrm{n}}}$	Ratio of true surface area over nominal surface area	–	Y	El-Soudani (1978)
S_{p}	$S_{\mathrm{p}} = \frac{1}{n}\sum_{i=1}^{n} S_{\mathrm{p},i}$	Mean peak spacing	Y	–	Whitehouse (1994)
S_{m}	$S_{\mathrm{m}} = \frac{1}{n}\sum_{i=1}^{n} S_{\mathrm{m},i}$	Mean zero-width spacing	–	–	Whitehouse (1994) and ISO (1997)
$R_{\Delta a}$	$R_{\Delta a} = \frac{1}{L}\int_0^L \left\lvert \frac{\mathrm{d}z(x)}{\mathrm{d}x} \right\rvert \mathrm{d}x$	Average slope	Y	–	Whitehouse (1994)
$R'_{\Delta a}$	$R'_{\Delta a} = \frac{1}{L}\int_0^L \left\lvert \frac{\mathrm{d}^2z(x)}{\mathrm{d}x^2} \right\rvert \mathrm{d}x$	Average curvature	Y	–	Whitehouse (1994)
$R_{\lambda q}$	$R_{\lambda q} = \frac{2\pi R_q}{R_{\Delta q}}$	Average wavelength	Y	–	Spragg and Whitehouse (1970, 1972)

Table 1 (continued)

Variable	Formula	Description	2D program	3D program	Sources
$p(z)$	Amplitude density of $z(x)$	Amplitude density function	Y	–	Whitehouse (1994) and ISO (1997)
$P(z)$	$P(z) = \int_0^z p(z)\mathrm{d}z$	Cumulative amplitude density function	Y	–	Whitehouse (1994)
ACVF(τ)	$\mathrm{ACVF}(\tau) = \lim_{L\to\infty} \frac{1}{L}\int_0^L z(x)z(x+\tau)\mathrm{d}x$	Autocovariance function of the profile with lag distance τ	Y	–	Sayles and Thomas (1977) and Thomas (1981)
ACF(τ)	$\mathrm{ACF}(\tau) = \frac{\mathrm{ACVF}(\tau)}{R_q^2}$	Autocorrelation function of the profile with lag distance τ	Y	–	Sayles and Thomas (1977) and Thomas (1981)
SF(τ)	$\mathrm{SF}(\tau) = \lim_{L\to\infty} 1/L\int_L [z(x) - z(x+\tau)]^2\mathrm{d}x = 2R_q^2[1-\mathrm{ACF}(\tau)]$	Structure function of the profile with lag distance τ	Y	–	Sayles and Thomas (1977)
$D, A, S(w)$	$S(w) = Aw^H$ $S(w) = \mathrm{RMS}(w) = \frac{1}{n_w}\sum_{i=1}^{n_w} \sqrt{\frac{1}{m_i-2}\sum_{j\in w_i}(z_j-\bar{z})^2}$	Roughness-length method fractal characterization	Y	Y	Malinverno (1990), Kulatilake et al. (1998), Lanaro (2000) and Fardin et al. (2001)
$G(f)$	$G(f) = \lim_{L\to\infty}\frac{1}{L}\left\lvert\int_0^L z(x)\mathrm{e}^{-\mathrm{i}2\pi fx}\mathrm{d}x\right\rvert^2$ $G(f) = Cf^{-\beta}$	Power spectral density from profile and fractal characterization	Y	–	Sayles and Thomas (1978), Berry and Lewis (1980); Brown and Scholz (1985), Brown (1987) and Power and Tullis (1991)
H	$\sigma(\Delta x) = \alpha(\Delta x)^H$ $\sigma(\Delta x) = \sqrt{\frac{1}{N}\sum_L \lvert z(x) - z(x+\Delta x)\rvert^2}$	Root-mean-square correlation fractal characterization	–	–	Renard et al. (2006) and Candela et al. (2009)
$\theta^*_{\max}/(C+1)$	$\tan\theta^* = -\tan\theta\cos\alpha$ $A_{\theta^*} = A_0\left(\frac{\theta^*_{\max}-\theta^*}{\theta^*_{\max}}\right)^C$	Directional roughness metric	Y	Y	Grasselli et al. (2002), Grasselli and Egger (2003) and Tatone and Grasselli (2009)

Appendix 2

To alleviate the time and effort put into processing roughness, a calculator application was developed as an open-source package by the authors implementing most of the methods discussed in this work (Table 1). The software and source code are open-source and can be obtained at the Geomechanics Group @ University of Toronto website (http://www.geogroup.utoronto.ca/?ddownload=5130). Statistical parameters are immediately calculated and are typically the fastest to process. Functional characterizations are displayed on graphs that can be generated then saved by the user. More complex characterization methods using fractal theory or shear-dependency tend to take a large amount of time depending on the number of points used. Further analysis on the outputs can be done as all raw data is output into text files and input surfaces are rotated and translated to align their mean plane along the x–y plane.

Synthetic surface roughness is also implemented based on the power spectrum methodology described in Sect. 5.1.3 (Brown 1995; Candela et al. 2009). A computer generated pseudo-random seed is used to generate a 3D square surface complying with user-specified Hurst exponents along the x- and y-axes based on the code by Candela et al. (2009). Afterwards, the surface elevation is scaled down to match a target R_q value and the spacing between points scaled to match a user-requested length. The 3D surface can be saved and triangulated for input using the Delaunay triangulation algorithm. For 2D profiles, a slice can be selected from the surface along either the x- or y- axis and placed in the import queue for processing (Fig. 14).

Before attempting to use 3D characterization methods, the surface mesh should be inspected for any holes, gaps, and non-useful features. Cropping the surface may be necessary to ensure that the mesh is contiguous. It is recommended to use a third-party STL viewer such as GOM Inspect (GOM 2018) or MeshLab (Cignoni et al. 2008) prior to processing the data to ensure data quality. Understanding 3D characterization methods is important to ensure that the results given are not of poor quality as the results would have no indication of such. Surface roughness fractal characterization using the roughness length method and the directional roughness characterization is computationally demanding. The implementations for both methods are briefly described below.

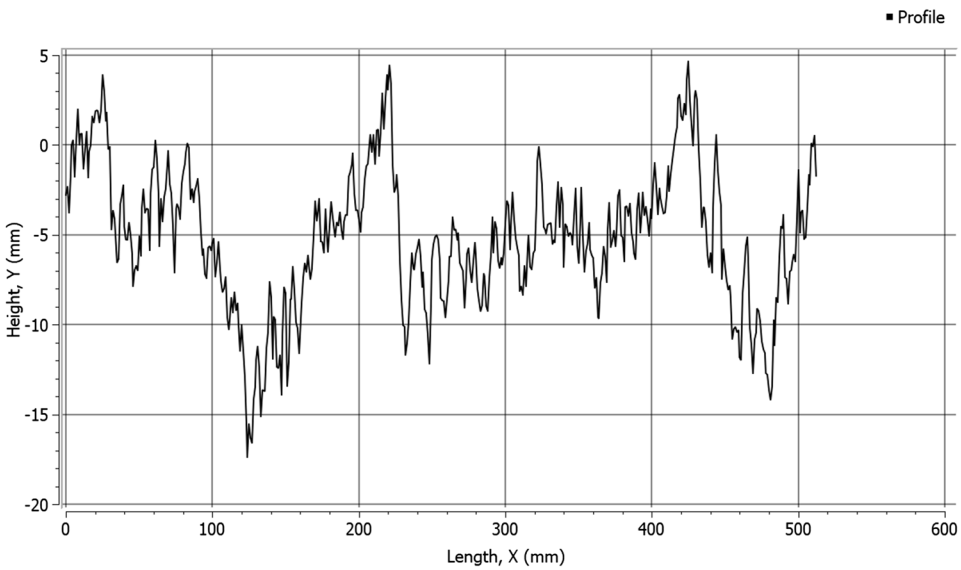

Fig. 14 Synthetic profile generated in the program using the algorithm presented by Candela et al. (2009)

2.1 Fractal Characterization: Roughness Length Method

The roughness length method requires a range of specified "window sizes" on which the surface is analyzed. These windows are divisions of the surface as discussed in Sect. 3.1. Although window sizes can be specified, the actual windows themselves are sized to capture the minimum and maximum vertices along the x- and y-axes. This is done by dividing the surface with a set number of windows along the shortest side of the surface bounding box (defined by the minimum and maximum x- and y-axis coordinates) then dividing the surface accordingly. The windows are aligned based on the reference system given and along the bounding box of the surface.

2.2 Directional Roughness Characterization

In evaluating the directional roughness of a surface, the potentially contacting facets are determined by the difference between the triangle facet normal and the direction of shear (Eq. 25). Some differences to the mathematical description of the apparent dip angle used for calculation of potential contact areas are necessary. While Eq. (25) can be applied to each triangular facet of the 3D surface, reliance on trigonometric functions should be reduced especially with calculations sensitive to rotation. To provide a more consistent approach to calculating the apparent dip angle, the relationship

$$\cos\left(\theta^{*}+90^{\circ}\right)=\frac{\left[\boldsymbol{n}-\mathrm{proj}_{\boldsymbol{t}_{\mathrm{norm}}}(\boldsymbol{n})\right]}{\left\|\left[\boldsymbol{n}-\mathrm{proj}_{\boldsymbol{t}_{\mathrm{norm}}}(\boldsymbol{n})\right]\right\|}\cdot\boldsymbol{t} \tag{39}$$

is used, where $\boldsymbol{n}$ is the triangle facet normal vector, $\boldsymbol{t}$ is the analysis direction vector and $\boldsymbol{t}_{\mathrm{norm}}$ is the vector normal to the analysis direction plane, and $\mathrm{proj}_{\boldsymbol{t}_{\mathrm{norm}}}$ is the projection function against $\boldsymbol{t}_{\mathrm{norm}}$. This equation provides mathematically equivalent results to Eq. (25) but with more robust computation than trigonometric functions.

After determining the apparent dip angle of each triangular facet, the triangle areas are binned by the apparent dip angle to obtain a cumulative distribution on which Eq. 26 can be fitted. A non-linear fitting method is required since logarithmic transformation of the equation yields a

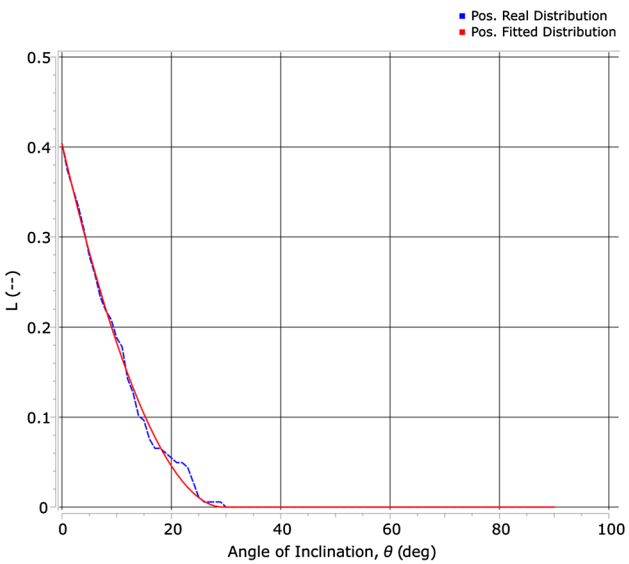

Fig. 15 Directional roughness distribution for a 2D profile along the positive direction

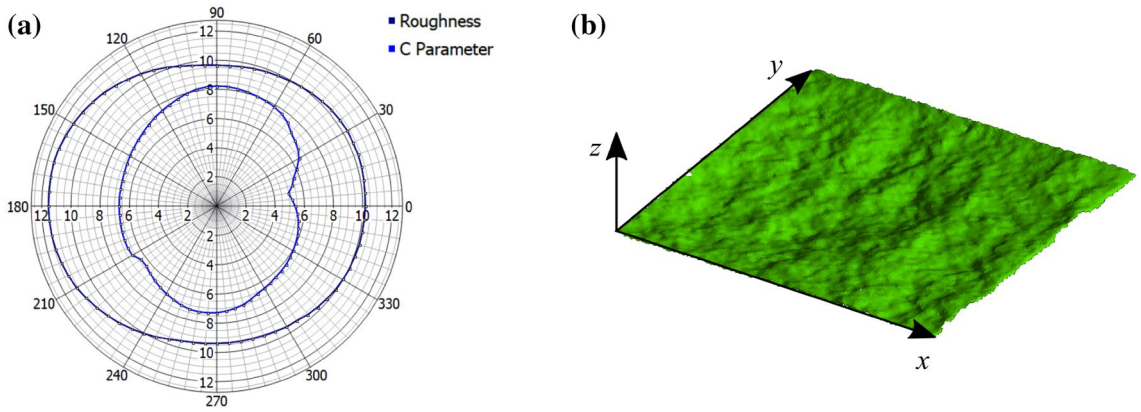

Fig. 16 **a** Directional roughness is plotted along with the *C* parameter in the middle of the plot. **b** The surface analyzed can be imaged in 3D with basic functionality

non-linear relationship (Tatone and Grasselli 2009). As such, the Gauss–Newton fitting algorithm (Björck 1996) was directly implemented for the cumulative distribution fitting curve. The fitting process is iterative and is stopped once the change in the calculated value is less than a user-defined threshold.

2.3 Graphical Output

In addition to providing the results of roughness data using the various methods, the program can provide graphical imaging of data. Graphical imaging for 2D profiles is more developed due to the simplicity of 2D characterization. These graphs provide a view of the fitting performed to provide some quality assurance of the resultant parameters. Amplitude density characterization is immediately comparable with the provided profile and can be used to visually judge the validity of the obtained statistical parameters (Fig. 2). The apparent angle distribution and fitting for the directional roughness method is also provided to ensure the quality of the fitting (Fig. 15). Fractal roughness characterization with the roughness-length method is plotted along with the regression function. The autocovariance function, autocorrelation function, and structure function are also provided graphically. Finally, the PSD can be viewed either with respect to wavelength (Fig. 6) or wavenumber.

Graphical presentation in 3D does not have the same variety of graphs that the 2D version produces, but its usefulness is best shown with directional characterization. Radial plots can be generated to see the directional change in roughness and the roughness metric's components (Fig. 16a) and a 3D graphic of a surface can be produced given that the computer's rendering capabilities are sufficient (Fig. 16b).

References

Ban L, Zhu C, Qi C, Tao Z (2018) New roughness parameters for 3D roughness of rock joints. Bull Eng Geol Environ. https://doi.org/10.1007/s10064-018-1394-3

Barnsley MF, Devaney RL, Mandelbrot BB, Peitgen H-O, Saupe D, Voss RF (1988) The science of fractal images. Springer, New York

Barton N (1973) Review of a new shear-strength criterion for rock joints. Eng Geol 7:287–332. https://doi.org/10.1016/0013-7952(73)90013-6

Barton N, Choubey V (1977) The shear strength of rock joints in theory and practice. Rock Mech Rock Eng 10:1–54. https://doi.org/10.1007/BF01261801

Barton N, Bandis S, Bakhtar K (1985) Strength, deformation and conductivity coupling of rock joints. Int J Rock Mech Min 22:121–140. https://doi.org/10.1016/0148-9062(85)93227-9

Beer AJ, Stead D, Coggan JS (2002) Technical note estimation of the joint roughness coefficient (JRC) by visual comparison. Rock Mech Rock Eng 35:65–74. https://doi.org/10.1007/s006030200009

Belem T, Homand-Etienne F, Souley M (2000) Quantitative parameters for rock joint surface roughness. Rock Mech Rock Eng 33:217–242. https://doi.org/10.1007/s006030070001

Bendat JS (1980) Engineering applications of correlation and spectral analysis. Wiley, New York

Berry MV, Hannay JH (1978) Topography of random surfaces. Nature 273:573. https://doi.org/10.1038/273573a0

Berry MV, Lewis ZV (1980) On the Weierstrass–Mandelbrot fractal function. Proc R Soc A Math Phys Eng Sci 370:459–484. https://doi.org/10.1098/rspa.1980.0044

Bhushan B (2000) Surface roughness analysis and measurement techniques. In: Bhushan B (ed) Modern tribology handbook, two volume set. CRC Press, Boca Raton

Bhushan B, Israelachvili JN, Landman U (1995) Nanotribology: friction, wear and lubrication at the atomic scale. Nature 374:607–616. https://doi.org/10.1038/374607a0

Björck A (1996) Numerical methods for least squares problems. SIAM, Philadelphia

Brown SR (1987) A note on the description of surface roughness using fractal dimension. Geophys Res Lett 14:1095–1098. https://doi.org/10.1029/GL014i011p01095

Brown SR (1995) Simple mathematical model of a rough fracture. J Geophys Res Solid Earth 100:5941–5952. https://doi.org/10.1029/94JB03262

Brown SR, Scholz CH (1985) Broad bandwidth study of the topography of natural rock surfaces. J Geophys Res 90:12575–12852. https://doi.org/10.1029/JB090iB14p12575

Brown SR, Scholz CH (1986) Closure of rock joints. J Geophys Res 91:4939–4948. https://doi.org/10.1029/JB091iB05p04939

Brown SR, Kranz RL, Bonner BP (1986) Correlation between the surfaces of natural rock joints. Geophys Res Lett 13:1430–1433. https://doi.org/10.1029/GL013i013p01430

Busse A, Lützner M, Sandham ND (2015) Direct numerical simulation of turbulent flow over a rough surface based on a surface scan. Comput Fluids 116:129–147. https://doi.org/10.1016/j.compfluid.2015.04.008

Candela T, Renard F, Bouchon M, Brouste A, Marsan D, Schmittbuhl J, Voisin C (2009) Characterization of fault roughness at various scales: implications of three-dimensional high resolution topography measurements. Pure Appl Geophys 166:1817–1851. https://doi.org/10.1007/s00024-009-0521-2

Chae BG, Chida Y, Jeong GC, Seo YS, Kim BC (2004) Roughness measurement of rock discontinuities using a confocal laser scanning microscope and the Fourier spectral analysis. Eng Geol 72:181–199. https://doi.org/10.1016/j.enggeo.2003.08.002

Cignoni P, Callieri M, Corsini M, Dellepiane M, Ganovelli F, Ranzuglia G (2008) MeshLab: an open-source mesh processing tool. In: Eurographics Italian chapter conference. The Eurographics Association, pp 129–136

Cottrell B (2009) Updates to the GG-shear strength criterion. M. Eng. thesis, University of Toronto

Cottrell B, Tatone BSA, Grasselli G (2010) Joint replica shear testing and roughness degradation measurement. In: ISRM-EUROCK-2010-043. International society for rock mechanics and rock engineering, ISRM, p 4

Crandall D, Bromhal G, Karpyn ZT (2010) Numerical simulations examining the relationship between wall-roughness and fluid flow in rock fractures. Int J Rock Mech Min 47:784–796. https://doi.org/10.1016/j.ijrmms.2010.03.015

Dieterich JH, Kilgore BD (1994) Direct observation of frictional contacts: new insights for state-dependent properties. Pure Appl Geophys 143:283–302. https://doi.org/10.1007/BF00874332

Dight PM, Chiu HK (1981) Prediction of shear behaviour of joints using profiles. Int J Rock Mech Min 18:369–386. https://doi.org/10.1016/0148-9062(81)90002-4

El-Soudani SM (1978) Profilometric analysis of fractures. Metallography 11:247–336. https://doi.org/10.1016/0026-0800(78)90045-9

Fardin N (2008) Influence of structural non-stationarity of surface roughness on morphological characterization and mechanical deformation of rock joints. Rock Mech Rock Eng 41:267–297. https://doi.org/10.1007/s00603-007-0144-9

Fardin N, Stephansson O, Jing L (2001) The scale dependence of rock joint surface roughness. Int J Rock Mech Min 38:659–669. https://doi.org/10.1016/S1365-1609(01)00028-4

Fardin N, Feng Q, Stephansson O (2004) Application of a new in situ 3D laser scanner to study the scale effect on the rock joint surface roughness. Int J Rock Mech Min 41:329–335. https://doi.org/10.1016/S1365-1609(03)00111-4

Gadelmawla ES, Koura MM, Maksoud TMA, Elewa IM, Soliman HH (2002) Roughness parameters. J Mater Process Technol 123:133–145. https://doi.org/10.1016/S0924-0136(02)00060-2

Gallant JC, Moore ID, Hutchinson MF, Gessler P (1994) Estimating fractal dimension of profiles: a comparison of methods. Math Geol 26:455–481. https://doi.org/10.1007/BF02083489

Ge Y, Kulatilake PHSW, Tang H, Xiong C (2014) Investigation of natural rock joint roughness. Comput Geotech 55:290–305. https://doi.org/10.1016/j.compgeo.2013.09.015

Gentier S, Riss J, Archambault G, Flamand R, Hopkins D (2000) Influence of fracture geometry on shear behaviour. Int J Rock Mech Min 37:161–174. https://doi.org/10.1016/S1365-1609(99)00096-9

Glover PWJ, Matsuki K, Hikima R, Hayashi K (1998) Synthetic rough fractures in rocks. J Geophys Res Solid Earth 103:9609–9620. https://doi.org/10.1029/97JB02836

GOM (2018) GOM Inspect. GOM

Grasselli G, Egger P (2003) Constitutive law for the shear strength of rock joints based on three-dimensional surface parameters. Int J Rock Mech Min 40:25–40. https://doi.org/10.1016/S1365-1609(02)00101-6

Grasselli G, Wirth J, Egger P (2002) Quantitative three-dimensional description of a rough surface and parameter evolution with shearing. Int J Rock Mech Min 39:789–800. https://doi.org/10.1016/S1365-1609(02)00070-9

Hurst HE (1951) Long-term storage capacity of reservoirs. Trans Am Soc Civil Eng 116:770–799

International Organization for Standardization (1996) Geometrical product specifications (GPS)—surface texture: profile method—metrological characteristics of phase correct filters (ISO/DIS standard no. 11562)

International Organization for Standardization (1997) Geometrical product specifications (GPS)—surface texture: profile method—terms, definitions and surface texture parameters. (ISO/DIS standard no. 4287)

International Organization for Standardization (2010) Geometrical product specifications (GPS)—surface texture: areal—part 6: classification of methods for measuring surface texture (ISO/DIS standard no. 25178-6)

International Organization for Standardization (2012) Geometrical product specifications (GPS)—surface texture: areal—part 2: terms, definitions and surface texture parameters (ISO/DIS Standard No. 25178-2)

ISRM (1978) International society for rock mechanics commission on standardization of laboratory and field tests: suggested methods for the quantitative description of discontinuities in rock masses. Int J Rock Mech Min 15:319–368. https://doi.org/10.1016/0148-9062(78)91472-9

Jang H-S, Kang S-S, Jang B-A (2014) Determination of joint roughness coefficients using roughness parameters. Rock Mech Rock Eng 47:2061–2073. https://doi.org/10.1007/s00603-013-0535-z

Jing L, Nordlund E, Stephansson O (1992) An experimental study on the anisotropy and stress-dependency of the strength and deformability of rock joints. Int J Rock Mech Min 29:535–542. https://doi.org/10.1016/0148-9062(92)91611-8

Jing Y, Armstrong RT, Mostaghimi P (2017) Rough-walled discrete fracture network modelling for coal characterisation. Fuel 191:442–453. https://doi.org/10.1016/j.fuel.2016.11.094

Koyama T, Fardin N, Jing L, Stephansson O (2006) Numerical simulation of shear-induced flow anisotropy and scale-dependent aperture and transmissivity evolution of rock fracture replicas. Int J Rock Mech Min 43:89–106. https://doi.org/10.1016/j.ijrmms.2005.04.006

Krahn J, Morgenstern NR (1979) The ultimate frictional resistance of rock discontinuities. Int J Rock Mech Min 16:127–133. https://doi.org/10.1016/0148-9062(79)91449-9

Krohn CE, Thompson AH (1986) Fractal sandstone pores: automated measurements using scanning-electron-microscope images. Phys Rev B 33:6366–6374. https://doi.org/10.1103/PhysRevB.33.6366

Kulatilake PHSW, Um J (1999) Requirements for accurate quantification of self-affine roughness using the roughness-length method. Int J Rock Mech Min 36:5–18. https://doi.org/10.1016/S0148-9062(98)00170-3

Kulatilake PHSW, Shou G, Huang TH, Morgan RM (1995) New peak shear strength criteria for anisotropic rock joints. Int J Rock Mech Min 32:673–697. https://doi.org/10.1016/0148-9062(95)00022-9

Kulatilake PHSW, Um J, Pan G (1998) Requirements for accurate quantification of self-affine roughness using the variogram method. Int J Solids Struct 35:4167–4189. https://doi.org/10.1016/S0020-7683(97)00308-9

Lanaro F (2000) A random field model for surface roughness and aperture of rock fractures. Int J Rock Mech Min 37:1195–1210. https://doi.org/10.1016/S1365-1609(00)00052-6

Lanaro F, Stephansson O (2003) A unified model for characterisation and mechanical behaviour of rock fractures. Pure Appl Geophys 160:989–998

Liu Q, Tian Y, Liu D, Jiang Y (2017) Updates to JRC-JCS model for estimating the peak shear strength of rock joints based on quantified surface description. Eng Geol 228:282–300. https://doi.org/10.1016/j.enggeo.2017.08.020

Liu Q, Tian Y, Ji P, Ma H (2018) Experimental investigation of the peak shear strength criterion based on three-dimensional surface description. Rock Mech Rock Eng 51:1005–1025. https://doi.org/10.1007/s00603-017-1390-0

Maerz NH, Franklin JA, Bennett CP (1990) Joint roughness measurement using shadow profilometry. Int J Rock Mech Min 27:329–343. https://doi.org/10.1016/0148-9062(90)92708-M

Mah J, Samson C, McKinnon SD, Thibodeau D (2013) 3D laser imaging for surface roughness analysis. Int J Rock Mech Min 58:111–117. https://doi.org/10.1016/j.ijrmms.2012.08.001

Malinverno A (1990) A simple method to estimate the fractal dimension of a self-affine series. Geophys Res Lett 17:1953–1956. https://doi.org/10.1029/GL017i011p01953

Mandelbrot B (1967) how long is the coast of Britain? Statistical self-similarity and fractional dimension. Science 156:636–638. https://doi.org/10.1126/science.156.3775.636

Mandelbrot B (1982) The fractal geometry of nature. W.H. Freeman, San Francisco

Mandelbrot B (1985) Self-affine fractals and fractal dimension. Phys Scr 32:257–260. https://doi.org/10.1088/0031-8949/32/4/001

Matsuki K, Chida Y, Sakaguchi K, Glover PWJ (2006) Size effect on aperture and permeability of a fracture as estimated in large synthetic fractures. Int J Rock Mech Min 43:726–755. https://doi.org/10.1016/j.ijrmms.2005.12.001

McCraw C, Edlmann K, Miocic J, Gilfillan S, Haszeldine RS, McDermott CI (2016) Experimental investigation and hybrid numerical analytical hydraulic mechanical simulation of supercritical CO_2 flowing through a natural fracture in caprock. Int J Greenh Gas Control 48:120–133. https://doi.org/10.1016/j.ijggc.2016.01.002

Myers NO (1962) Characterization of surface roughness. Wear 5:182–189. https://doi.org/10.1016/0043-1648(62)90002-9

Odling NE (1994) Natural fracture profiles, fractal dimension and joint roughness coefficients. Rock Mech Rock Eng 27:135–153. https://doi.org/10.1007/BF01020307

Ogilvie SR, Isakov E, Glover PWJ (2006) Fluid flow through rough fractures in rocks. II: A new matching model for rough rock fractures. Earth Planet Sci Lett 241:454–465. https://doi.org/10.1016/j.epsl.2005.11.041

Olsson WA, Brown SR (1993) Hydromechanical response of a fracture undergoing compression and shear. Int J Rock Mech Min 30:845–851. https://doi.org/10.1016/0148-9062(93)90034-B

Poon CY, Sayles RS, Jones TA (1992) Surface measurement and fractal characterization of naturally fractured rocks. J Phys D Appl Phys 25:1269–1275. https://doi.org/10.1088/0022-3727/25/8/019

Power WL, Tullis TE (1991) Euclidean and fractal models for the description of rock surface roughness. J Geophys Res 96:415–424. https://doi.org/10.1029/90JB02107

Power WL, Tullis TE, Brown SR, Boitnott GN, Scholz CH (1987) Roughness of natural fault surfaces. Geophys Res Lett 14:29–32. https://doi.org/10.1029/GL014i001p00029

Power WL, Tullis TE, Weeks JD (1988) Roughness and wear during brittle faulting. J Geophys Res Solid Earth 93:15268–15278. https://doi.org/10.1029/JB093iB12p15268

Rabinowicz E (1956) Autocorrelation analysis of the sliding process. J Appl Phys 27:131–135. https://doi.org/10.1063/1.1722321

Rathmann U (2014) QwtPolar—a Qwt/Qt Polar Plot Library

Rathmann U, Wilgen J (2016) Qwt— Qt Widgets for Technical Applications

Raven KG, Gale JE (1985) Water flow in a natural rock fracture as a function of stress and sample size. Int J Rock Mech Min 22:251–261. https://doi.org/10.1016/0148-9062(85)92952-3

Reeves MJ (1985) Rock surface roughness and frictional strength. Int J Rock Mech Min 22:429–442. https://doi.org/10.1016/0148-9062(85)90007-5

Renard F, Voisin C, Marsan D, Schmittbuhl J (2006) High resolution 3D laser scanner measurements of a strike-slip fault quantify its morphological anisotropy at all scales. Geophys Res Lett. https://doi.org/10.1029/2005GL025038

Sagy A, Brodsky EE, Axen GJ (2007) Evolution of fault-surface roughness with slip. Geology 35:283–286. https://doi.org/10.1130/G23235A.1

Sanderson C, Curtin R (2016) Armadillo: a template-based C++ library for linear algebra. J Open Source Softw 1:26. https://doi.org/10.21105/joss.00026

Sayles RS, Thomas TR (1977) The spatial representation of surface roughness by means of the structure function: a practical alternative to correlation. Wear 42:263–276. https://doi.org/10.1016/0043-1648(77)90057-6

Sayles RS, Thomas TR (1978) Surface topography as a nonstationary random process. Nature 271:431–434. https://doi.org/10.1038/271431a0

Shirono T, Kulatilake PHSW (1997) Accuracy of the spectral method in estimating fractal/spectral parameters for self-affine roughness profiles. Int J Rock Mech Min 34:789–804. https://doi.org/10.1016/S1365-1609(96)00068-X

Spragg RC, Whitehouse DJ (1970) A new unified approach to surface metrology. Proc Inst Mech Eng 185:697–707. https://doi.org/10.1243/PIME_PROC_1970_185_081_02

Spragg RC, Whitehouse DJ (1972) An average wavelength parameter for surface metrology. Meas Control 5:95–101. https://doi.org/10.1177/002029407200500301

Tang ZC, Wong LNY (2016) New criterion for evaluating the peak shear strength of rock joints under different contact states. Rock Mech Rock Eng 49:1191–1199. https://doi.org/10.1007/s00603-015-0811-1

Tatone BSA (2009) Quantitative characterization of natural rock discontinuity roughness in-situ and in the laboratory. MASc thesis, University of Toronto

Tatone BSA, Grasselli G (2009) A method to evaluate the three-dimensional roughness of fracture surfaces in brittle geomaterials. Rev Sci Instrum 80:125110. https://doi.org/10.1063/1.3266964

Tatone BSA, Grasselli G (2010) A new 2D discontinuity roughness parameter and its correlation with JRC. Int J Rock Mech Min 47:1391–1400. https://doi.org/10.1016/j.ijrmms.2010.06.006

Tatone BSA, Grasselli G (2012) Quantitative measurements of fracture aperture and directional roughness from rock cores. Rock Mech Rock Eng 45:619–629. https://doi.org/10.1007/s00603-011-0219-5

Tatone BSA, Grasselli G (2013) An investigation of discontinuity roughness scale dependency using high-resolution surface measurements. Rock Mech Rock Eng 46:657–681. https://doi.org/10.1007/s00603-012-0294-2

Tatone BSA, Grasselli G, Cottrell B (2010) Accounting for the influence of measurement resolution on discontinuity roughness estimates.

In: ISRM international symposium-EUROCK 2010. International Society for Rock Mechanics
The Qt Company (2018) Qt development framework. The Qt Company, Helsinki
Thomas TR (1981) Characterization of surface roughness. Precis Eng 3:97–104. https://doi.org/10.1016/0141-6359(81)90043-X
Tian Y, Liu Q, Liu D, Kang Y, Deng P, He F (2018) Updates to Grasselli's peak shear strength model. Rock Mech Rock Eng. https://doi.org/10.1007/s00603-018-1469-2
Tse R, Cruden DM (1979) Estimating joint roughness coefficients. Int J Rock Mech Min 16:303–307. https://doi.org/10.1016/0148-9062(79)90241-9
Whitehouse DJ (1994) Handbook of surface metrology. Institute of Physics Pub, Philadelphia
Whitehouse DJ (1997) Surface metrology. Meas Sci Technol 8:955
Whitehouse DJ, Archard JF (1970) The properties of random surfaces of significance in their contact. Proc R Soc Lond A 316:97–121. https://doi.org/10.1098/rspa.1970.0068
Witherspoon PA, Wang JSY, Iwai K, Gale JE (1980) Validity of Cubic Law for fluid flow in a deformable rock fracture. Water Resour Res 16:1016–1024. https://doi.org/10.1029/WR016i006p01016
Wong P (1987) Fractal surfaces in porous media. AIP, New York, pp 304–317
Xia C-C, Tang Z-C, Xiao W-M, Song Y-L (2014) New peak shear strength criterion of rock joints based on quantified surface description. Rock Mech Rock Eng 47:387–400. https://doi.org/10.1007/s00603-013-0395-6
Yang ZY, Lo SC, Di CC (2001) Reassessing the joint roughness coefficient (JRC) estimation using Z2. Rock Mech Rock Eng 34:243–251. https://doi.org/10.1007/s006030170012
Yang J, Rong G, Hou D, Peng J, Zhou C (2016) Experimental study on peak shear strength criterion for rock joints. Rock Mech Rock Eng 49:821–835. https://doi.org/10.1007/s00603-015-0791-1
Yeo IW, de Freitas MH, Zimmerman RW (1998) Effect of shear displacement on the aperture and permeability of a rock fracture. Int J Rock Mech Min 35:1051–1070. https://doi.org/10.1016/S0148-9062(98)00165-X
Yu X, Vayssade B (1991) Joint profiles and their roughness parameters. Int J Rock Mech Min 28:333–336. https://doi.org/10.1016/0148-9062(91)90598-G
Zhao Q, Tisato N, Kovaleva O, Grasselli G (2018) Direct observation of faulting by means of rotary shear tests under X-ray micro-computed tomography. J Geophys Res Solid Earth. https://doi.org/10.1029/2017JB015394
Zimmerman RW, Bodvarsson GS (1996) Hydraulic conductivity of rock fractures. Transport Porous Med 23:1–30. https://doi.org/10.1007/BF00145263